EFFECTS OF VISCOSITY AND CONSTRAINTS ON THE DISPERSION AND DISSIPATION OF WAVES IN LARGE BLOOD VESSELS

I. Theoretical Analysis

EVERETT JONES, MAX ANLIKER, *and* I-DEE CHANG

From the Department of Aeronautics and Astronautics, Stanford University, Stanford, California 94305, and the Ames Research Center of the National Aeronautics and Space Administration, Moffett Field, California 94035

ABSTRACT The propagation of sounds and pulse waves within the cardiovascular system is subject to strong dissipative mechanisms. To investigate the effects of blood viscosity on dissipation as well as dispersion of small waves in arteries and veins, a parametric study has been carried out. A linearized analysis of axisymmetric waves in a cylindrical membrane that contains a viscous fluid indicates that there are two families of waves: a family of slow waves and one of fast waves. The faster waves are shown to be more sensitive to variations in the elastic properties of the medium surrounding the blood vessels and at high values of the frequency parameter α defined by $\alpha = \sqrt{\rho\omega R_0^2/\mu}$ the blood viscosity attenuates them more strongly over a length than the slow waves. At low values of α, the effects of viscosity on attenuation are reversed; that is, the family of slow waves is much more attenuated than the family of fast waves. For the slow waves the radial displacement component generally exceeds the axial component except at very low frequencies. Conversely the axial displacements are much larger than the radial displacement for the faster waves. The presence of external constraints, however, can modify these results. In the case of the slow waves the phase angle between pressure and radial wall displacement is virtually negligible in the presence of mild external constraints, while the phase angles between pressure and fluid mass flow are at most 45°. The corresponding phase angles for the fast waves exhibit much larger variations with changes in the elastic properties of the surrounding medium.

I. INTRODUCTION

Physiological Considerations

A quantitative analysis of the dynamics of the circulatory system is considerably more formidable than similar investigations of most engineering systems. The blood

itself is a non-newtonian fluid that exhibits the characteristics of solutions and colloidal and particle suspensions. Controlled experiments (1) have shown that the apparent viscosity increases with hematocrit, decreases with strain rate, and has a viscosity coefficient that ranges from 1 centipoise to 10 poise. McDonald (2), however, reports that blood in the larger arteries and veins behaves like a newtonian fluid and normally has a viscosity coefficient of approximately 4–7 centipoise. No marked manifestations of non-newtonian behavior are observed in large blood vessels. Even though blood exhibits compressibility, it has negligible effects on the transmission properties of the usual types of waves that may occur in blood vessels (3–5).

The experiments of Bergel (6) and those of McDonald and Gessner (7) indicate that the blood vessel walls are viscoelastic with material properties that depend more strongly on strain than strain rate. Also, blood vessels are essentially incompressible and, therefore, have a Poisson's ratio of approximately 0.5 (2). Experimental data (2) further indicate that the modulus of elasticity for the artery varies from about 10^6 to 10^8 dynes/cm^2. The viscoelastic modulus (imaginary part of the complex modulus) can be of the order of 25% of the elastic modulus (real part) (6, 7). Geometrically, the larger blood vessels are tapered tubes with the ratio of wall thickness/radius ranging from about 0.08 to 0.30 for arteries and from about 0.01 to 0.05 for veins. There is also evidence that the walls of blood vessels exhibit anisotropy (8) and nonlinear stress-strain relationships (9). The blood vessels are imbedded in tissues, muscle, or bone and are usually constrained by these surroundings. Their effects upon the wave transmission characteristics have not yet been studied extensively and only limited quantitative data are available (10).

Previous Theoretical Investigations

Numerous theoretical studies of the dynamic behavior of blood vessels have been reported in the literature. Comprehensive reviews of such investigations have been made by McDonald (2), Rudinger (11), Skalak (12), and Fung (13). The complexities of the physical and geometric features of blood vessels necessitate an approximate approach in any analysis of their motion. By introducing simplifying yet realistic assumptions and a mathematical model for the mechanical behavior of the vessels, it is possible to arrive at a tractable analytical formulation of dynamic problems such as the prediction of the dispersion and attenuation of waves.

The theoretical analyses of dynamic problems of blood vessels can be separated into two major groups on the basis of the relative rigor with which the solid or fluid mechanics aspects have been treated. Recent contributions emphasizing a realistic formulation of the fluid-dynamic aspects were made by Morgan and Kiely (14), Womersley (15), Atabek and Lew (16), and Atabek (17). The work presented here is an extension of these efforts and is based on a similar mathematical model.

The analytical model introduced by Morgan and Kiely (14) treats the vessel wall

as a linear elastic, homogeneous, isotropic, cylindrical membrane free of constraints and assumes that the blood behaves like an incompressible newtonian fluid in laminar motion. Womersley (15) also used this model but added a distributed, axial, elastic constraint acting on the outside surface of the vessel to approximate the effects of the surrounding medium. The analyses by Morgan and Kiely (14) and by Womersley (15) have become key references. In both studies the wave reflections were neglected and only one type of wave was considered. The corresponding solution is not sufficiently general to accommodate constraints such as those enforced by branches and bifurcations or by the application of instruments such as electromagnetic flowmeters. A further inadequacy of the Womersley solution (15) manifests itself whenever distributed radial constraints are present. Womersley's results (15) predict at most a 15% change in the speed of the wave studied for arbitrary variations in the axial constraint and for all $\alpha = \sqrt{\rho\omega R_0^2/\mu}$. By contrast, the addition of an infinite radial constraint besides an infinite axial constraint produces a rigid tube incapable of transmitting waves when filled with an incompressible fluid. It appears, therefore, that radial constraint may play an important role and should be taken into consideration.

Atabek and Lew (16) investigated the effects of initial stresses upon the propagation characteristics of two types of waves. An extension of this analysis by Atabek (17) took into consideration the influences of radial and axial constraints and anisotropic wall behavior; however, results were presented only for special examples which do not illustrate the relative significance of axial and radial constraints.

In a parametric study of waves in blood vessels, Maxwell and Anliker (3–5) treated the blood as an inviscid, compressible fluid and assumed the vessel wall to behave like a cylindrical shell with viscoelastic wall properties. In contrast to a membrane model, the shell model exhibits resistance to local bending in the vessel wall and thus allows the study of a wider class of motions by relaxing the restriction to very small changes in the radii of curvature. The effects of initial stresses are taken into account but external constraints are disregarded. Three wave types were predicted. For both axially symmetric and nonaxially symmetric mode shapes, the waves were characterized by the dominant displacement component that an arbitrary point of the middle surface exhibits at higher frequencies and are accordingly referred to as radial, circumferential, and axial waves. The properties of the axially symmetric radial waves are in agreement with Womersley's results (15) for very small fluid viscosity, and the predicted speeds of axially symmetric radial and axial waves are basically compatible with the results of Atabek and Lew (16) for the inviscid limit.

Intent and Scope of This Analysis

The main objective of the present theoretical analysis is a parametric study of the effects of blood viscosity, distributed external constraints, and viscoelastic proper-

ties of the vessel on the transmission characteristics of radial and axial waves. To this end, a mathematical model is introduced which is similar to those in references 4–6. It differs from them by the inclusion of radial constraints and by considering the vessel wall to be viscoelastic.

The arrangement of this report reflects the actual sequence of the studies conducted. In section II, the boundary value problem is derived and linearized with emphasis upon the main conditions of linearization. Section III is devoted to the general solution. The results of the parametric analysis for the transmission characteristics, including velocity profiles, are described in section IV.

II. THE LINEARIZED BOUNDARY VALUE PROBLEM

The basic problem of interest is the motion of a blood vessel and the blood it contains when this system is subjected to an oscillatory perturbation; however, only the motion of a model of this system is actually analyzed. A steady-state configuration (Fig. 1) consisting of a long, cylindrical tube containing a streaming newtonian fluid is perturbed such that axially symmetric motion with no circumferential velocity is obtained. The perturbation is assumed to be sufficiently small to justify linearization. Therefore, all dependent variables can be expressed in the form

$$(\ ) = (\ )_s + (\ )' \qquad (1)$$

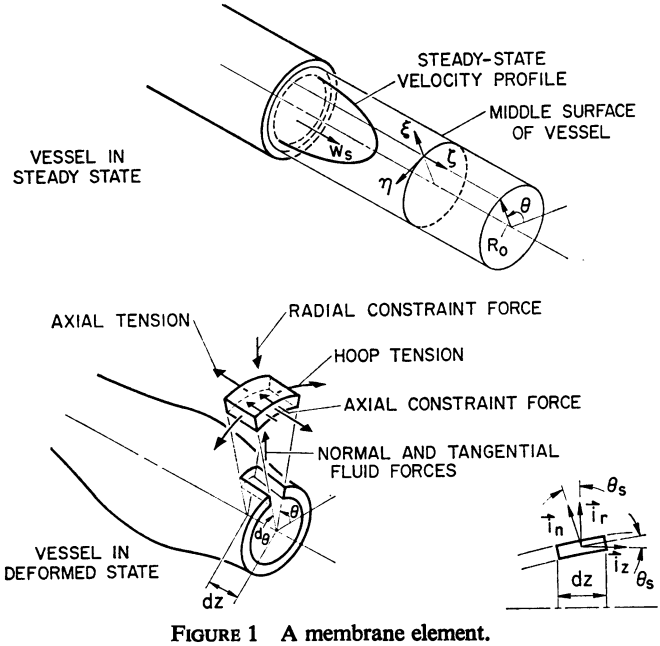

FIGURE 1 A membrane element.

where

( ) = the value of a variable in the perturbed state,
$(\ )_s$ = the value of a variable in the steady state,
$(\ )'$ = the perturbation of the variable.

Since the desired boundary value problem is linear, harmonic solutions for a given frequency can be obtained and more general motions can be studied using Fourier synthesis.

The wall material is assumed to be isotropic, homogeneous, and elastic. Furthermore, the tube is assumed to have a wall thickness/radius ratio

$$\frac{h}{R_0} \ll 1, \tag{2}$$

and to behave like a membrane with constant strains and stresses across the wall. Since the problem is axially symmetric, the wall displacements, stresses, and strains are functions only of axial distance and time. To render the membrane assumption realistic, the displacements will be limited to those producing very small changes in the radii of curvature. This is achieved with the restriction.

$$\frac{L}{R_0} \gg 1, \tag{3}$$

where L is any characteristic axial dimension.

For 0 mean flow and no initial stresses the equations of motion for the vessel wall in the presence of radial and axial constraints can be given in the form

$$\rho_w h \frac{\partial^2 \xi}{\partial t^2} = -K_1 \xi + (p')_{r=R_0} - \frac{Eh}{R_0(1-\sigma^2)}\left(\frac{\xi}{R_0} + \sigma \frac{\partial \zeta}{\partial z}\right), \tag{4}$$

$$\rho_w h \frac{\partial^2 \zeta}{\partial t^2} = -K_2 \zeta - \mu \left(\frac{\partial w}{\partial r}\right)_{r=R_0} + \frac{Eh}{1-\sigma^2}\left(\frac{\partial^2 \zeta}{\partial z^2} + \frac{\sigma}{R_0}\frac{\partial \xi}{\partial z}\right) \tag{5}$$

These equations differ from those given by Womersley by the inclusion of a radial constraint term $-K_1\xi$. K_1 and K_2 are measures of the elastic or viscoelastic (K_1 and K_2 complex) restraining effects of the surrounding medium on the radial and axial wall motions. Reference 10 shows that this kind of model is indeed approximate, at least for the axial wall displacement and frequencies above 1 Hz. The linearized differential equations for the fluid flow are

$$\frac{1}{r}\frac{\partial r u'}{\partial r} + \frac{\partial w'}{\partial z} = 0, \tag{6}$$

$$\frac{\partial w'}{\partial t} = -\frac{1}{\rho}\frac{\partial p'}{\partial z} + \frac{\nu}{r}\frac{\partial}{\partial r}\left(r\frac{\partial w'}{\partial r}\right), \tag{7}$$

$$0 = \frac{\partial p'}{\partial r} \tag{8}$$

and the boundary conditions can be expressed as

$$u'(R_0, z, t) = \frac{\partial \xi}{\partial t}(z, t), \quad w'(R_0, z, t) = \frac{\partial \zeta}{\partial t}(z, t). \tag{9}$$

A detailed derivation of this system of equations is given in reference 18.

III. SOLUTION OF THE LINEARIZED BOUNDARY VALUE PROBLEM

The General Solution

The complete linearized boundary value problem is given by equations 4–9. By differentiating equation 7 with respect to r and making use of equation 8, one obtains

$$\rho\frac{\partial}{\partial t}\left(\frac{\partial w'}{\partial r}\right) = \mu\frac{\partial}{\partial r}\left[\frac{1}{r}\frac{\partial}{\partial r}\left(r\frac{\partial w'}{\partial r}\right)\right]. \tag{10}$$

For the axially symmetric case $(\partial\omega'/\partial r)_{r=0} = 0$, which means that no purely oscillatory term in $\partial\omega'/\partial r$ is possible. Therefore, a separable harmonic solution can be given in the form

$$\frac{\partial w'}{\partial r} = R(r)Z_1(z)e^{i\omega t}. \tag{11}$$

The substitution of equation 11 into equation 10 yields

$$\frac{i\omega}{\nu}R(r) = \frac{\mathrm{d}}{\mathrm{d}r}\left\{\frac{1}{r}\frac{\mathrm{d}}{\mathrm{d}r}[rR(r)]\right\}.$$

Changing the independent variable using

$$bs = r, \quad \text{where } \frac{1}{b} = \sqrt{-\frac{\omega}{i\nu}} = i^{3/2}\sqrt{\frac{\omega}{\nu}}, \tag{12}$$

leads to

$$\frac{\mathrm{d}^2R(r)}{\mathrm{d}s^2} + \frac{1}{s}\frac{\mathrm{d}R(r)}{\mathrm{d}s} + \left(1 - \frac{1}{s^2}\right)R(r) = 0,$$

which is Bessel's equation for functions of order 1. The general solution of this equation is

$$R(r) = AJ_1\left(\frac{r}{b}\right) + BY_1\left(\frac{r}{b}\right);$$

however, substitution of this into equation 11 and application of the symmetry requirement, $(\partial\omega'/\partial r)_{r=0} = 0$ yields $B = 0$ and

$$\frac{\partial w'}{\partial r} = Z_1(z)J_1\left(\frac{r}{b}\right)e^{i\omega t}, \tag{13}$$

or, after integration,

$$w'(r, z, t) = \left\{Z_1(z)b\left[1 - J_0\left(\frac{r}{b}\right)\right] + i\omega F_1(z)\right\}e^{i\omega t}. \tag{14}$$

Substitution of equation 14 into equation 7 gives an oscillatory expression for $\partial p'/\partial z$ which can also be integrated and expressed in the form

$$p'(z, t) = \frac{\mu}{b}\left[Z(z) + \frac{i\omega}{b}F(z) + F_2\right]e^{i\omega t}, \tag{15}$$

where

$$Z_1(z) = Z'(z) = \frac{dZ(z)}{dZ}, F_1(z) = F'(z) = \frac{dF(z)}{dz}. \tag{16}$$

From equations 14 and 16, it follows that

$$w'(r, z, t) = \left\{\left[1 - J_0\left(\frac{r}{b}\right)\right]Z'(z) + \frac{i\omega}{b}F'(z)\right\}be^{i\omega t}. \tag{17}$$

By substituting equation 17 into equation 6 and integrating with respect to r one obtains

$$u'(r, z, t) = b\left\{\left[bJ_1\left(\frac{r}{b}\right) - \frac{r}{2}\right]Z''(z) - \frac{r}{2}\frac{i\omega}{b}F''(z)\right\}e^{i\omega t}, \tag{18}$$

where the function of z and t generated by this integration must vanish since $u'(r, z, t)$ vanishes for $r = 0$.

The expressions for $\partial\xi/\partial t$ and $\partial\zeta/\partial t$ given by equations 9, 17, and 18 can be integrated with respect to time to yield the oscillatory solution

$$\xi(z, t) = R_0\left\{\frac{b}{i\omega}\left[\frac{b}{R_0}J_1\left(\frac{R_0}{b}\right) - \frac{1}{2}\right]Z''(z) - \frac{1}{2}F''(z)\right\}e^{i\omega t}, \tag{19}$$

$$\zeta(z, t) = \left\{\frac{b}{i\omega}\left[1 - J_0\left(\frac{R_0}{b}\right)\right] Z'(z) + F'(z)\right\} e^{i\omega t}. \quad (20)$$

According to equation 17 the unsteady mass flux can be written in first approximation

$$Q'(z, t) = \int_0^{R_0} \rho w'(r, z, t) 2\pi r \, dr = \left\{\left[\frac{1}{2} - \frac{b}{R_0} J_1\left(\frac{R_0}{b}\right)\right] Z'(z) + \frac{1}{2}\frac{i\omega}{b} F'(z)\right\} 2\pi R_0^2 \rho b e^{i\omega t}. \quad (21)$$

Substitution of equations 15, 17, 19, and 20 into equations 4 and 5 leads to

$$\frac{i\omega}{b}[A_4 R_0^2 F''(z) - \beta_1 F(z)] = A_3 R_0^2 Z''(z) + \beta_1 Z(z) + \beta_1 F_2, \quad (22)$$

$$\frac{i\omega}{b}\left[\beta_3\left(1 - \frac{\sigma}{2}\right) R_0^2 F'''(z) + (1 - \Gamma_2) F'(z)\right] A_2 R_0^2 Z'''(z) - A_1 Z'(z), \quad (23)$$

where

$$\Gamma_1 = \frac{K_1}{\rho_w h \omega^2}, \Gamma_2 = \frac{K_2}{\rho_w h \omega^2}, \beta_1 = \frac{\rho R_0}{\rho_w h}, \beta_2 = \frac{C_0}{R_0 \omega}, \quad (24)$$

$$\beta_3 = \frac{E}{\rho_w R_0^2 \omega^2 (1 - \sigma^2)} = \frac{2\beta_1 \beta_2^2}{(1 - \sigma^2)}, \alpha = \sqrt{\frac{\omega}{\nu}} R_0, C_0^2 = \frac{Eh}{2\rho R_0}, \quad (25)$$

$$A_1 = (1 - \Gamma_2)[1 - J_0(i^{3/2}\alpha)] - \beta_1 \frac{i^{-3/2}}{\alpha} J_1(i^{3/2}\alpha), \quad (26)$$

$$A_2 = -\beta_3\left\{[1 - J_0(i^{3/2}\alpha)] + \sigma\left[\frac{i^{-3/2}}{\alpha} J_1(i^{3/2}\alpha) - \frac{1}{2}\right]\right\}, \quad (27)$$

$$A_3 = (1 - \Gamma_1 - \beta_3)\left[\frac{i^{-3/2}}{\alpha} J_1(i^{3/2}\alpha) - \frac{1}{2}\right] - \beta_3\sigma[1 - J_0(i^{3/2}\alpha)], \quad (28)$$

$$A_4 = \tfrac{1}{2}(1 - \Gamma_1) - \beta_3(\tfrac{1}{2} - \sigma). \quad (29)$$

Elimination of $F'''(z)$ from equations 22 and 23 and integration of the resulting equation gives

$$\frac{i\omega}{b} F(z) = -\frac{A_6}{A_5} R_0^2 Z''(z) - \frac{A_7}{A_5} Z(z) + F_3, \quad (30)$$

where

$$A_5 = \beta_1 + \frac{A_4(1 - \Gamma_2)}{\beta_3(1 - \sigma/2)}, A_6 = A_3 - \frac{A_2 A_4}{\beta_3\left(1 - \frac{\sigma}{2}\right)}, A_7 = \beta_1 + \frac{A_1 A_4}{\beta_3\left(1 - \frac{\sigma}{2}\right)}. \quad (31)$$

By combining equations 30 and 22 one obtains

$$R_0^4 Z''''(z) + A_8 R_0^2 Z''(z) + A_9 Z(z) = -(F_2 + F_3)\frac{\beta_1 A_5}{A_4 A_6} \quad (32)$$

where

$$A_8 = \left[A_7 + \frac{A_3(1 - \Gamma_2) + \beta_1 A_2}{\beta_3(1 - \sigma/2)}\right]/A_6, \quad (33)$$

$$A_9 = \frac{1 - \Gamma_2 - A_1\beta_1}{\beta_3(1 - \sigma/2)\,A_6}. \quad (34)$$

Equation 32 then has the general solution

$$Z(z) = [D_1 e^{-\sqrt{B_1}z/R_0} + D_2 e^{\sqrt{B_1}z/R_0}] + [D_3 e^{-\sqrt{B_2}z/R_0} + D_4 e^{\sqrt{B_2}z/R_0}] - (F_2 + F_3)\frac{\beta_1 A_5}{A_4 A_6 A_9}, \quad (35)$$

where B_1 and B_2 are the roots of the equation

$$B^2 + A_8 B + A_9 = 0,$$

$$B_1 = \tfrac{1}{2}[-A_8 + (A_8^2 - 4A_9)^{1/2}], \qquad B_2 = -\tfrac{1}{2}[A_8 + (A_8^2 - 4A_9)^{1/2}]. \quad (36)$$

From equations 35 and 30 one finds

$$\frac{i\omega}{b}F(z) = -\frac{(A_6 B_1 + A_7)}{A_5}[D_1 e^{-\sqrt{B_1}z/R_0} + D_2 e^{\sqrt{B_1}z/R_0}] - \frac{(A_6 B_2 + A_7)}{A_5}[D_3 e^{-\sqrt{B_2}z/R_0} + D_4 e^{\sqrt{B_2}z/R_0}] + (F_2 + F_3)\frac{\beta_1 A_7}{A_4 A_6 A_9} + F_3. \quad (37)$$

Substitution of equations 35 and 37 into equations 15 and 17–20 completes the

formal solution. The resulting expression for p' can be given as

$$p'(z, t) = \frac{\mu}{b}\{S_1[D_1e^{-\sqrt{B_1}z/R_0} + D_2e^{\sqrt{B_1}z/R_0}] + S_2[D_3e^{-\sqrt{B_2}z/R_0} + D_4e^{\sqrt{B_2}z/R_0}]\}\, e^{i\omega t} \quad (38)$$

where

$$S_1 = 1 - \left(\frac{A_6B_1 + A_7}{A_5}\right), \quad S_2 = 1 - \left(\frac{A_6B_2 + A_7}{A_5}\right). \quad (39)$$

The pressure pulse is often resolved into its Fourier components in studying wave motion. Therefore, it is most convenient to write p' in the form

$$\begin{aligned} p'(z, t) &= p_1(z, t) + p_2(z, t) + p_3(z, t) + p_4(z, t), \\ p_1(z, t) &= P_1e^{i\omega(t-z/C_1)}\, e^{-\delta_1 z/R_0}, p_2(z, t) = P_2e^{i\omega(t+z/C_1)}\, e^{\delta_1 z/R_0}, \\ p_3(z, t) &= P_3e^{i\omega(t-z/C_2)}\, e^{-\delta_2 z/R_0}, p_4(z, t) = P_4e^{i\omega(t+z/C_2)}\, e^{\delta_2 z/R_0}, \end{aligned} \quad (40)$$

where

$$\frac{P_1}{D_1} = \frac{\mu}{b}S_1 = \frac{P_2}{D_2}, \quad \frac{P_3}{D_3} = \frac{\mu}{b}S_2 = \frac{P_4}{D_4}, \quad (41)$$

$$\frac{C_0}{C_1} = \beta_2 Im(\sqrt{B_1}), \delta_1 = Re(\sqrt{B_1}), \frac{C_0}{C_2} = \beta_2 Im(\sqrt{B_2}), \delta_2 = Re(\sqrt{B_2}). \quad (42)$$

It is also convenient to express the other quantities such that the phase relationship with respect to the pressure waves is exhibited. Substitution of equations 35, 37, 41, and 42 into equations 17–21 yields

$$w'(r, z, t) = \frac{-i}{\rho\omega R_0}\left\{\frac{\sqrt{B_1}}{S_1}\left[S_1 - J_0\left(i^{3/2}\alpha\frac{r}{R_0}\right)\right][p_1(z, t) - p_2(z, t)] + \frac{\sqrt{B_2}}{S_2}\left[S_2 - J_0\left(i^{3/2}\alpha\frac{r}{R_0}\right)\right][p_3(z, t) - p_4(z, t)]\right\}, \quad (43)$$

$$u'(r, z, t) = \frac{i}{\rho\omega R_0}\left\{\frac{B_1}{S_1}\left[\frac{i^{-3/2}}{\alpha}J_1\left(i^{3/2}\alpha\frac{r}{R_0}\right) - \frac{S_1}{2}\frac{r}{R_0}\right][p_1(z, t) + p_2(z, t)] + \frac{B_2}{S_2}\left[\frac{i^{-3/2}}{\alpha}J_1\left(i^{3/2}\alpha\frac{r}{R_0}\right) - \frac{S_2}{2}\frac{r}{R_0}\right][p_3(z, t) + p_4(z, t)]\right\}, \quad (44)$$

$$\xi(z, t) = \frac{1}{\rho\omega^2 R_0}\{[p_1(z, t) + p_2(z, t)]\, M_1e^{i\phi_1} + [p_3(z, t) + p_4(z, t)]\, M_2e^{i\phi_2}\}, \quad (45)$$

$$\zeta(z, t) = \frac{1}{\rho\omega^2 R_0}\{[p_1(z, t) - p_2(z, t)]\, M_3 e^{i\phi_3} + [p_3(z, t) - p_4(z, t)]\, M_4 e^{i\phi_4}\}, \quad (46)$$

$$Q'(z, t) = \frac{R_0}{\omega}\{[p_1(z, t) - p_2(z, t)]\, M_5 e^{i\phi_5} + [p_3(z, t) - p_4(z, t)]\, M_6 e^{i\phi_6}\}, \quad (47)$$

$$w'(0, z, t) = \frac{1}{\rho\omega R_0}\{[p_1(z, t) - p_2(z, t)]\, M_7 e^{i\phi_7} + [p_3(z, t) - p_4(z, t)]\, M_8 e^{i\phi_8}\}, \quad (48)$$

where

$$M_1 e^{i\phi_1} = -\frac{B_1}{S_1}\left[\frac{S_1}{2} - \frac{i^{-3/2}}{\alpha} J_1(i^{3/2}\alpha)\right],$$

$$M_2 e^{i\phi_2} = -\frac{B_2}{S_2}\left[\frac{S_2}{2} - \frac{i^{-3/2}}{\alpha} J_1(i^{3/2}\alpha)\right], \quad (49)$$

$$M_3 e^{i\phi_3} = -\frac{\sqrt{B_1}}{S_1}[S_1 - J_0(i^{3/2}\alpha)],\ M_4 e^{i\phi_4} = -\frac{\sqrt{B_2}}{S_2}[S_2 - J_0(i^{3/2}\alpha)], \quad (50)$$

$$M_5 e^{i\phi_5} = \frac{2\pi i}{\sqrt{B_1}} M_1 e^{i\phi_1},\ M_6 e^{i\phi_6} \frac{2\pi i}{\sqrt{B_2}} M_2 e^{i\phi_2}, \quad (51)$$

$$M_7 e^{i\phi_7} = -i\frac{\sqrt{B_1}}{S_1}(S_1 - 1),\ M_8 e^{i\phi_8} = -i\frac{\sqrt{B_2}}{S_2}(S_2 - 1). \quad (52)$$

Equations 40 and 43–52 are the solutions for fluid velocity, wall displacement, fluid mass flow, and fluid velocity on the axis as a function of time and position with six parameters (σ, β_1, β_2, α, Γ_1, and Γ_2) and four arbitrary constants (P_1, P_2, P_3, and P_4). This solution predicts four waves traveling in the axial direction. These four waves actually constitute only two different types of waves each with a transmitted wave (wave moving in the $+z$ direction) and a reflected wave (wave moving in the $-z$ direction). The waves of the same type are identical except for the direction of propagation. The four arbitrary constants determine the strength of the four waves.

The parameters σ and β_1 are functions only of physical and geometric properties of the fluid and the wall, while β_2 and α are functions of the physical and geometric properties and of the frequency. The external constraint parameters Γ_1 and Γ_2 reflect the character of the external constraints.

It is important to note that α has the form similar to the square root of an unsteady Reynolds number or

$$\alpha^2 = \frac{\omega}{\nu} R_0^2 = \frac{\rho(R_0\omega)R_0}{\mu}; \quad (53)$$

however, the velocity in this expression is not a fluid velocity and to avoid confusion α will not be referred to as a Reynolds number.

IV. NUMERICAL RESULTS FROM THE GENERAL SOLUTION

A Parametric Analysis

The wave speeds (C_1/C_0 and C_2/C_0), attenuation factors (δ_1 and δ_2), and the mode shapes (given by the magnitudes M_1–M_8) and phase angles (ϕ_1–ϕ_8) are of course functions only of the six parameters (σ, β_1, β_2, α, Γ_1, and Γ_2). The functional relationships, however, are complex and a parametric study is necessary to illustrate them. For the cardiovascular system, the geometric and physical parameters may be limited to

$$0.25 \leq \sigma \leq 0.5, \qquad 5 \leq \beta_1 \leq 20. \tag{54}$$

The range for β_2 and α should be as broad as possible but consistent with the long wavelength approximation which arises by applying equation 3 to wave motion.

$$\frac{\lambda_i}{R_0} = 2\pi\beta_2 \frac{C_i}{C_0} \gg 1, \text{ where } i = 1 \text{ or } 2. \tag{55}$$

Examination of results obtained for limiting forms of the solution for large constraints and large and small α, as in reference 18, demonstrates that Γ_1 and Γ_2 in the ranges

$$10^4 < \Gamma_1 < 10^7, \qquad \Gamma_2 < 6, \tag{56}$$

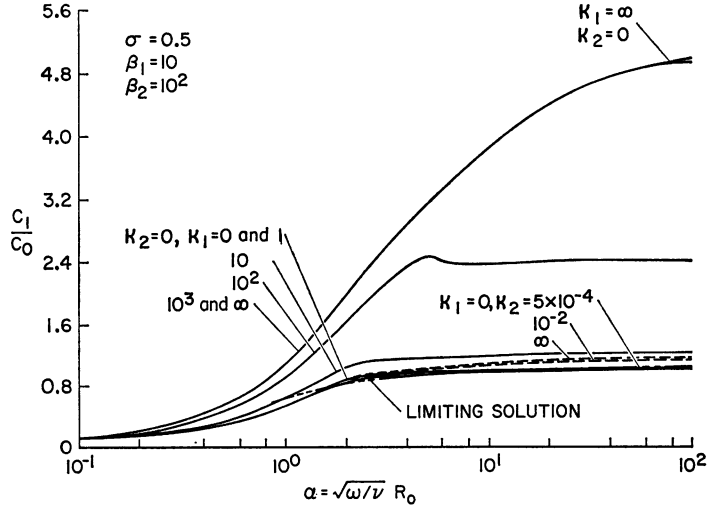

FIGURE 2 Wave speed for the first type of wave, C_1, as a function of α for different values of the constraint parameters κ_1 and κ_2. The limiting solution is only valid for large α and is shown only for $\beta_1 = 10$, $\beta_2 = 100$, $\sigma = \frac{1}{2}$, $\kappa_1 = \kappa_2 = 0$. (For derivation see part II, following paper.)

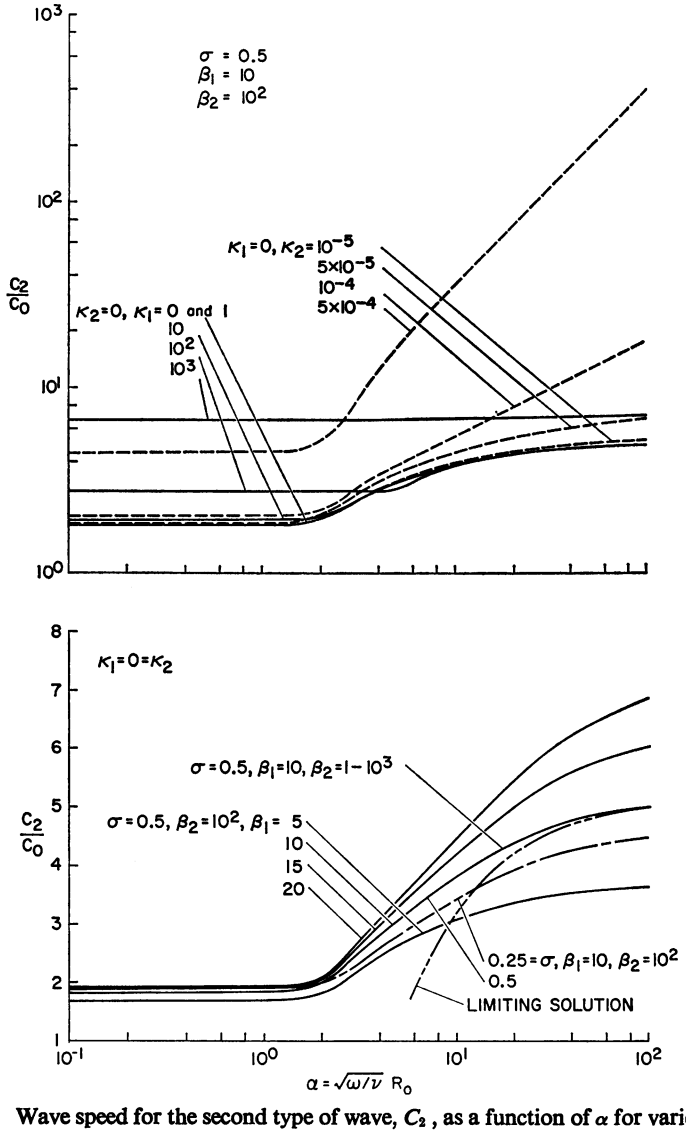

FIGURE 3 Wave speed for the second type of wave, C_2, as a function of α for various values of the parameters σ, β_1, β_2, κ_1, and κ_2.

produce the most significant effect upon the mathematical solution. Also, equation 55 will be satisfied for nominal cases if

$$\beta_2 > 1. \tag{57}$$

At the fundamental pulse frequency, β_2 is of the order 10^2. Since biological material is nearly incompressible, Poisson's ratio σ may be taken as 0.5. As a representative value for β_1, one may choose $\beta_1 = 10$. Therefore, the basic numerical values in the

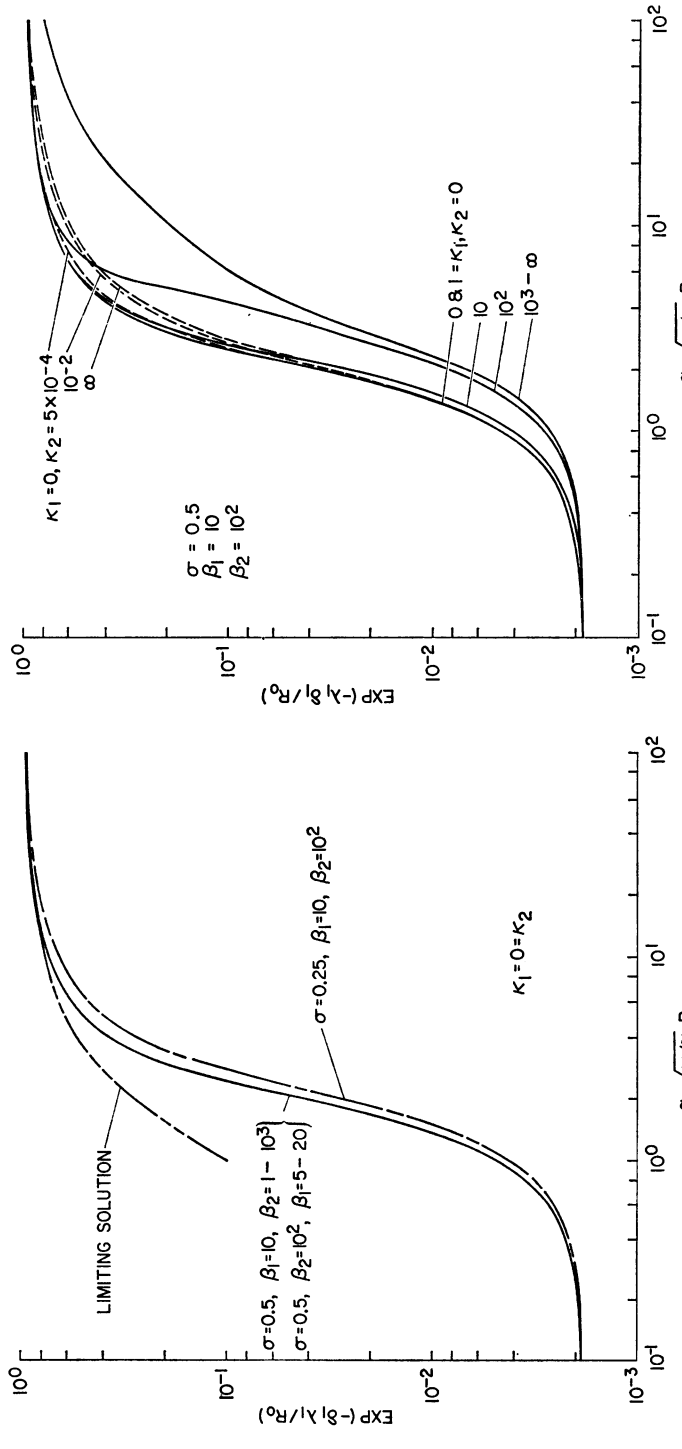

FIGURE 4 Transmission factor for the first type of wave as a function of α for various values of the parameters σ, β_1, β_2, κ_1, and κ_2.

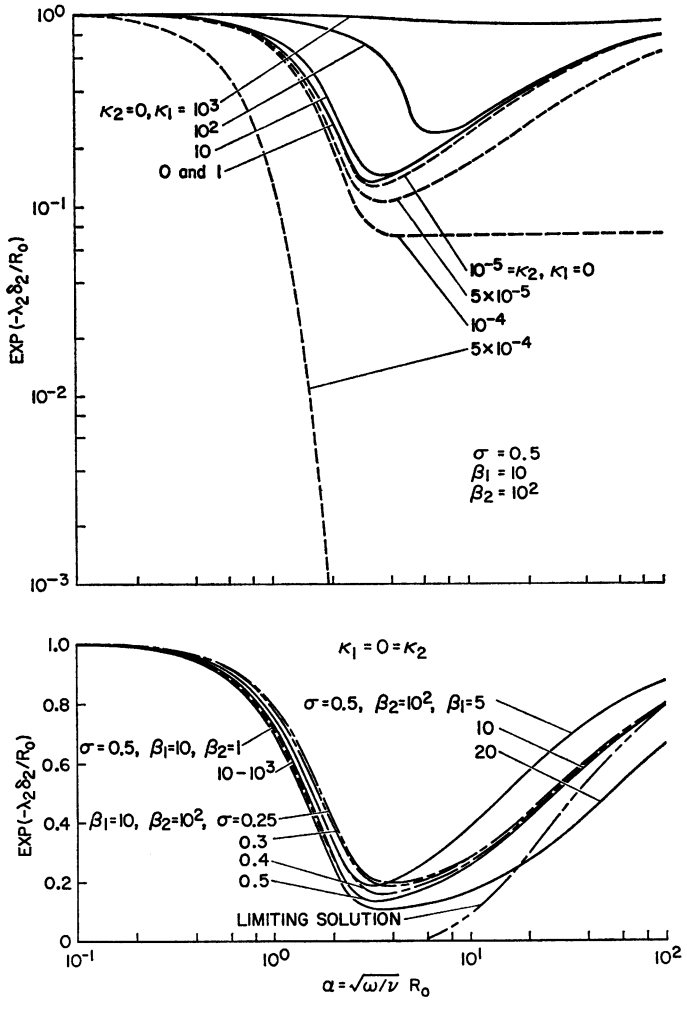

FIGURE 5 Transmission factor for the second type of wave as a function of α for various values of the parameters σ, β_1, β_2, κ_1, and κ_2.

parametric analysis were

$$\sigma = 0.5, \beta_1 = 10, \qquad \beta_2 = 10^2, \qquad \Gamma_1 = 0 = \Gamma_2 . \tag{58}$$

The constraint parameters Γ_1 and Γ_2 were modified for this study to reflect only the physical parameters of the system:

$$\kappa_1 = \frac{\Gamma_1}{\beta_2^2} = \frac{K_1 C_0^2}{\rho_w h R_0^2}, \qquad \kappa_2 = \frac{\Gamma_2}{\beta_2^2} = \frac{K_2 C_0^2}{\rho_w h R_0^2}. \tag{59}$$

In terms of these new constraint parameters, the basic numerical values defined by

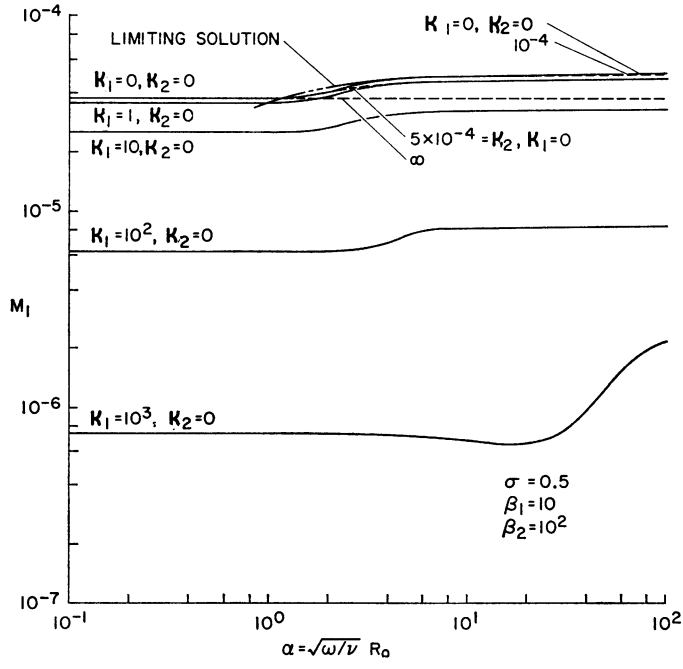

FIGURE 6 The mode shape coefficient M_1 for radial displacement of the first type of wave as a function of α for different values of the constraint parameters κ_1 and κ_2. The radial displacement for the first type of wave decreases with increasing radial constraint for all α and becomes asymptotically independent of α for increasing axial constraint.

equation 58 can now be given as

$$\sigma = 0.5, \quad \beta_1 = 10, \quad \beta_2 = 10^2, \quad \kappa_1 = 0 = \kappa_2, \tag{60}$$

and the most significant ranges for κ_1 and κ_2 for $\beta_2 = 10^2$ are

$$1 < \kappa_1 < 10^3, \quad \kappa_2 < 6 \times 10^{-4}. \tag{61}$$

Figs. 2–5 give the wave speeds and transmission factors. In this analysis the transmission factor is defined as $\exp(-\delta\lambda/R_0)$ which represents the ratio of the amplitude of a sinusoidal wave propagating over a distance of 1 wavelength to its initial value. Results corresponding to the limiting solutions valid for large values of α and $\beta_1 = 10$, $\beta_2 = 100$, $\sigma = \frac{1}{2}$, $\kappa_1 = \kappa_2 = 0$ (no constraints and elastic wall) are also shown in these figures as well as in Figs. 6–17 for comparison. The pertinent equations for the limiting solutions (large α) are given in part II (following paper) which describes the effects of a viscoelastic wall.

In general, the wave speed for the first type of wave increases monotonically with α from a small value at low α and approaches a finite limiting value. For weak radial constraint, it is relatively constant for $\alpha > 3$. Whenever the condition $(\lambda_1/R_0) = 2\pi\beta_2(c_1/c_0) \gg 1$ is satisfied, the parameters β_1 and β_2 have little effect

on this wave speed, and a change in Poisson's ratio σ has no significant effect at large α. For arbitrary values of κ_2 within the complete range of axial constraint ($0 \leq \kappa_2 \leq \infty$), the solution deviates at most by 15% from that corresponding to the basic values at all α; however, variations in the radial constraint produce marked changes particularly in the range $1 \leq \kappa_1 \leq 10^3$.

Except for cases with large radial constraints, the wave speed for the second type of wave is relatively constant at low α and increases monotonically with increasing α; however, changes in Poisson's ratio or β_1 produce much larger effects on the speed of this type of wave, while a variation in β_2 again has a negligible effect. According to this analysis the speed approaches infinity as α approaches infinity when either constraint parameter becomes unbounded; moreover in the presence of a radial constraint with $\kappa_1 > 10^3$ the wave speed is virtually independent of α.

The transmission factor for the first type of wave, exp $(-\delta_1\lambda_1/R_0)$, increases monotonically from 0 to 1 with α increasing from 0 to infinity. The parameters β_1 and β_2 have no effect, but a decrease in Poisson's ratio to 0.25 can produce a 30% decrease in transmission factor. Variations in the radial constraint ($0 \leq \kappa_1 \leq \infty$) may change the transmission factor by an order of magnitude. For α above 2, a change in axial constraint ($0 \leq \kappa_2 \leq \infty$) can alter the transmission factor by 30%.

For all cases with weak constraints, the transmission factor for the second type of wave is 1 for very large or very small α and has a minimum in the α range 3–5. β_1 has a very significant effect for α above 1, while Poisson's ratio has its most significant effect for α below 3. The transmission factor for the second type of wave is also unaffected by β_2. As shown in Fig. 5, this transmission factor *increases* with increasing radial constraint and decreases with increasing axial constraint. For $\kappa_2 \geq 5 \times 10^{-4}$, the transmission factor becomes negligible at large α.

Results for the mode shape coefficients M_1–M_6 and phase angles ϕ_1–ϕ_6 are shown on Figs. 6–17. The effects of σ, β_1, and β_2 on M_1 and M_5 are not shown graphically. Both M_1 and M_5 are independent of β_1. Also, M_5 is independent of σ while M_1 increases by only 32% for $\alpha < 2$ when σ decreases from 0.5 to 0.25. Furthermore, M_1 is inversely proportional to β_2^2 and M_5 is inversely proportional to β_2.

Figs. 6–17 show that the second type of wave has larger axial displacements in the basic parametric case than the first type of wave. Also, from Fig. 8 and the observation above, it follows that M_1 is inversely proportional to β_2^2 and M_3 is inversely proportional to β_2. Therefore, the ratio of radial/axial displacement (M_1/M_3) must become greater than 1 at a certain value of β_2. This change in the character of the mode shape is also observed in the inviscid limit and since β_2 is inversely proportional to the frequency, it implies that the first type of wave exhibits predominantly axial displacements at low frequencies (large β_2) and predominantly radial displacements at high frequencies (small β_2). The same behavior was predicted for inviscid fluids by Maxwell and Anliker (3–5).

For a given pressure variation the constraints may cause some interesting effects. With an increasing radial constraint the wave speed, attenuation, and axial dis-

placements for the first type of wave are generally increasing while radial displacements and mass flow rate decrease. On the other hand, the second type of wave exhibits an increase in wave speed and a decrease in attenuation, wall displacement, and fluid mass flow with increasing radial constraint. An increase in axial constraint causes an increase in speed and attenuation up to limiting values and a reduction in radial displacement, fluid mass flow, and axial displacement for the first type of wave, while for the second type of wave it produces an increase in the speed and attenuation.

The mode shape coefficients and phase angles generally exhibit an asymptotic behavior for small and large α. Therefore, in many cases of interest, an asymptotic solution may be sufficiently accurate.

It is interesting to note that at low α the phase angles ϕ_2, ϕ_3, ϕ_4, and ϕ_6 are very sensitive to deviations of σ from 0.5 and of κ_1 from 0. This prediction may be of value for the experimental determination of σ and κ_1.

Fluid Velocity Profiles

If only the incident wave of the first type occurs, then according to equations 43 and 44:

$$w_1'(r, z, t) = -\frac{i}{\rho\omega R_0}\frac{\sqrt{B_1}}{S_1}\left[S_1 - J_0\left(i^{3/2}\alpha\frac{r}{R_0}\right)\right]p_1(z, t),$$

$$u_1'(r, z, t) = \frac{i}{\rho\omega R_0}\frac{B_1}{S_1}\left[\frac{i^{-3/2}}{\alpha}J_1\left(i^{3/2}\alpha\frac{r}{R_0}\right) - \frac{S_1}{2}\frac{r}{R_0}\right]p_1(z, t).$$

These two equations can also be written in the form

$$\frac{w_1'(r, z, t)}{w_1'(0, z, t)} = \left[J_0\left(i^{3/2}\alpha\frac{r}{R_0}\right) - S_1\right]\Big/(1 - S_1), \tag{62}$$

$$\frac{u_1'(r, z, t)}{w_1'(0, z, t)} = \frac{\sqrt{B_1}}{1 - S_1}\left[\frac{i^{-3/2}}{\alpha}J_1\left(i^{3/2}\alpha\frac{r}{R_0}\right) - \frac{S_1}{2}\frac{r}{R_0}\right]. \tag{63}$$

Likewise, if only the incident wave of the second type occurs,

$$w_2'(r, z, t) = -\frac{i}{\rho\omega R_0}\frac{\sqrt{B_2}}{S_2}\left[S_2 - J_0\left(i^{3/2}\alpha\frac{r}{R_0}\right)\right]p_3(z, t),$$

FIGURE 7 The mode shape coefficient M_2 for radial displacement of the second type of wave as a function of α for various values of the parameters σ, β_1, β_2, κ_1, and κ_2. M_2 first decreases rapidly, attains a minimum, and then increases with increasing α. It varies significantly with Poisson's ratio for all α and with β_1 at larger α. Also, M_2 is inversely proportional to β_2^2. In the absence of constraints, $M_2/M_1 > 1$ for small α and $M_2/M_1 < 1$ for large α. M_2 decreases first at small α and then for all α with increasing radial constraint. With increasing axial constraint, M_2 decreases and then increases at large α.

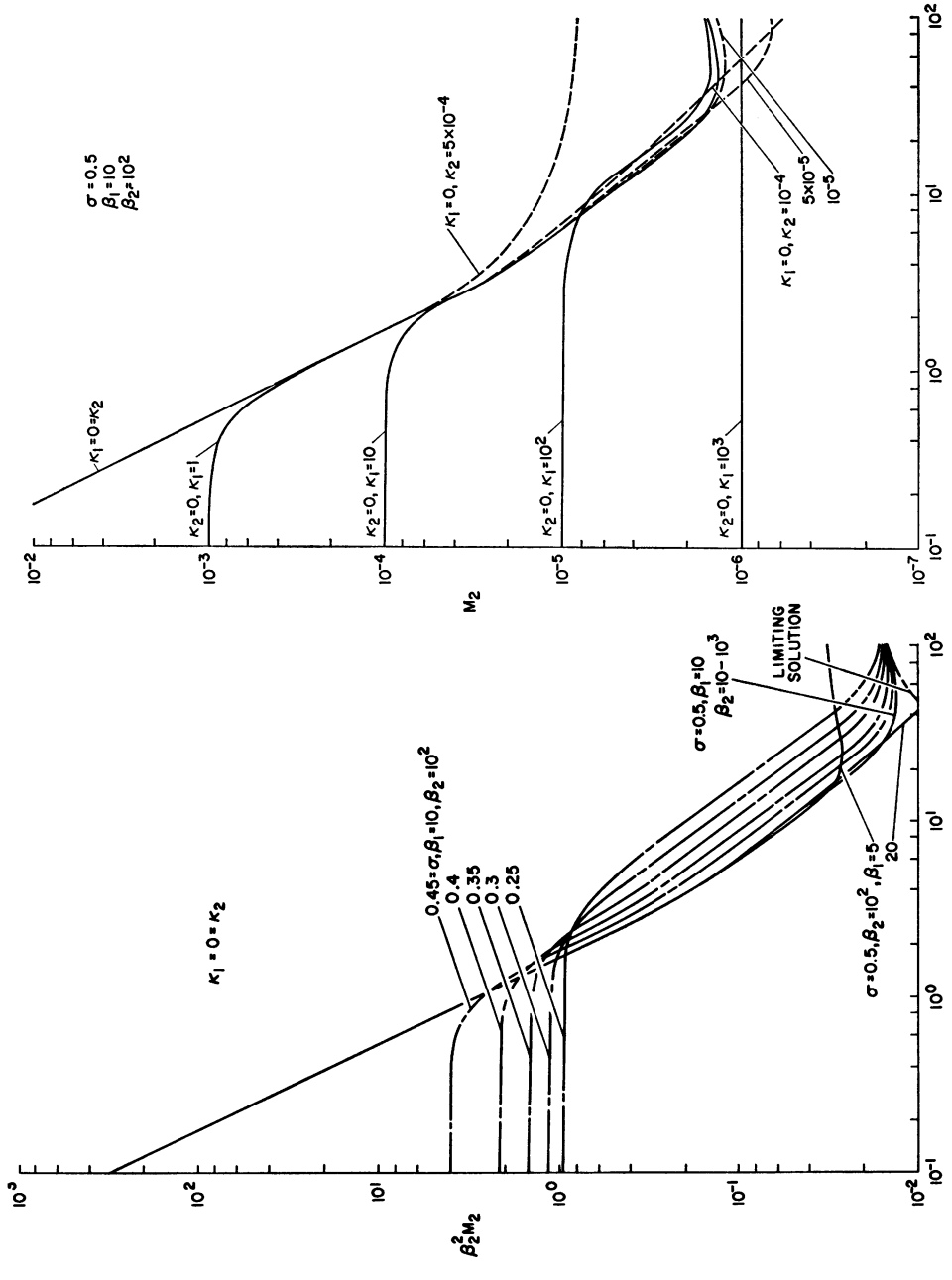
σ = 0.5
β1 = 10
β2 = 10²
κ1 = 0 = κ2
κ2 = 0, κ1 = 1
κ2 = 0, κ1 = 10
κ2 = 0, κ1 = 10²
κ2 = 0, κ1 = 10³
κ1 = 0, κ2 = 5×10⁻⁴
κ1 = 0, κ2 = 10⁻⁴
5×10⁻⁵
10⁻⁵
M2
α = √(ω/ν) R0
κ1 = 0 = κ2
0.45 = σ, β1 = 10, β2 = 10²
0.4
0.35
0.3
0.25
σ = 0.5, β1 = 10
β2 = 10 – 10³
LIMITING SOLUTION
σ = 0.5, β2 = 10², β1 = 5
20
β2²M2
α = √(ω/ν) R0

FIGURE 7

$$u_2'(r, z, t) = \frac{i}{\rho\omega R_0}\frac{B_2}{S_2}\left[\frac{i^{-3/2}}{\alpha}J_1\left(i^{3/2}\alpha\frac{r}{R_0}\right) - \frac{S_2}{2}\frac{r}{R_0}\right]p_3(z, t);$$

or

$$\frac{w_2'(r, z, t)}{w_2'(0, z, t)} = \left[J_0\left(i^{3/2}\alpha\frac{r}{R_0}\right) - S_2\right]\Big/(1 - S_2), \tag{64}$$

$$\frac{u_2'(r, z, t)}{w_2'(0, z, t)} = \frac{\sqrt{B_2}}{1 - S_2}\left[\frac{i^{-3/2}}{\alpha}J_1\left(i^{3/2}\alpha\frac{r}{R_0}\right) - \frac{S_2}{2}\frac{r}{R_0}\right], \tag{65}$$

For these simple waves, the expressions 62–65 are plotted in Figs. 18 and 19 for the basic case in the parametric analysis ($\sigma = 0.5$, $\beta_1 = 10$, $\beta_2 = 10^2$, $\kappa_1 = 0 = \kappa_2$) and three values of α. The axial velocity for the waves of the first type is generally largest in the center of the tube, but the difference between the magnitudes of the axial velocity on the axis and that on the wall decreases with increasing α. The magnitude of the radial velocity for the waves of the first type is largest near the tube wall, and its variation with r is greatest for low α. With increasing α the phase difference between the axial velocity at the tube wall and that on the tube axis decreases.

The most significant observation for the waves of the second type is that the change in magnitude and phase of the axial velocity across the tube is negligible at low α. This absence of an appreciable relative velocity at low α accounts for the small attenuation of waves of the second type. At higher α, the magnitude of the axial velocity at the tube wall is larger than at the axis. The difference in magnitude and phase for the axial velocity on the tube axis and on the tube wall increases with increasing α. For the radial velocity the variation in the magnitude across the tube is greatest and the difference in phase is least at low α.

Applications

To apply the analysis presented in the preceding sections to specific cases, the independent parameters α, β_1, β_2, σ, κ_1, and κ_2 must be prescribed. The wave propagation characteristics (wave speeds, attenuation factors, and mode shapes) can then be determined from the results given in the parametric analysis. The four arbitrary constants P_1, P_2, P_3, and P_4 appearing in the general solution are determined by satisfying four prescribed, independent conditions imposed on the dependent variables.

FIGURE 8 The mode shape coefficient M_3 for axial displacement of the first type of wave as a function of α for various values of the parameters σ, β_1, β_2, κ_1, and κ_2. M_3 increases rapidly at small α and approaches an asymptotic limit for large α. β_1 has an insignificant effect on M_3 but variations in M_3 due to Poisson's ratio can be significant. M_3 is inversely proportional to β_2. M_3 exhibits a small variation with axial constraint but depends strongly upon radial constraint for all α.

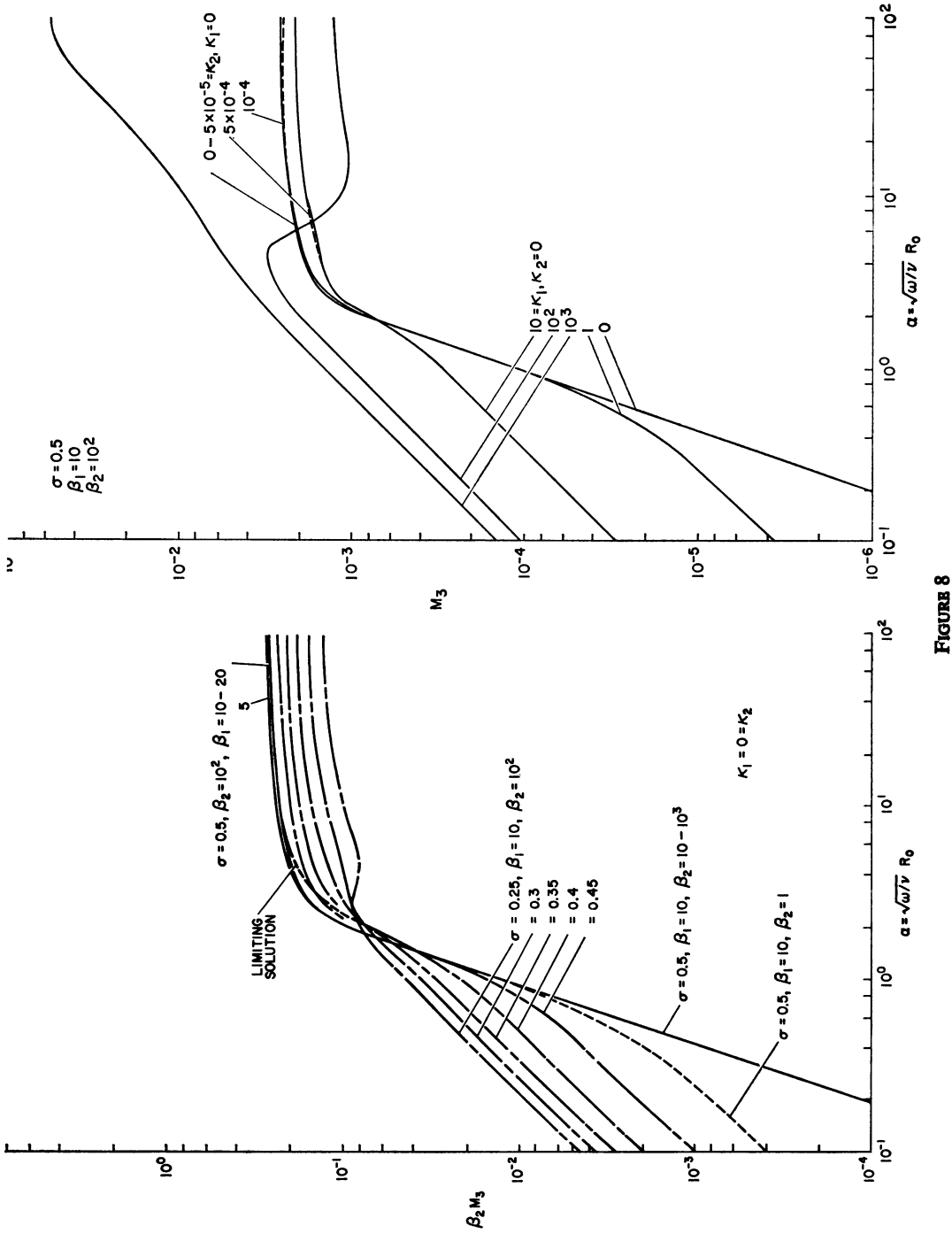
σ=0.5
β1=10
β2=10²
0-5×10⁻⁵=K2, K1=0
.5×10⁻⁴
10⁻⁴
10=K1, K2=0
10²
10³
1
0
M3
α=√(ω/ν) R0
σ=0.5, β2=10², β1=10-20
5
LIMITING SOLUTION
σ = 0.25, β1=10, β2=10²
= 0.3
= 0.35
= 0.4
= 0.45
σ=0.5, β1=10, β2=10-10³
K1 = 0=K2
σ=0.5, β1=10, β2=1
β2 M3

FIGURE 8

In the past many analyses have considered only the first type of wave using the solution given by Womersley (15). The analysis presented in this report allows for a separate study of each type of wave as well as for the general solution involving both types of waves. Besides this, it takes into account the effects of a distributed radial constraint in addition to those of a distributed axial constraint introduced by Womersley (15).

By considering only the first or radial type of wave ($P_{3R} = 0 = P_{4R}$), equations 40 and 42–48 reduce to

$$p_R(z, t) = P_{1R}e^{i\omega(t-z/C_1)}e^{-\delta_1 z/R_0} + P_{2R}e^{i\omega(t+z/C_1)}e^{\delta_1 z/R_0}, \tag{66}$$

$$Q'_R(z, t) = \frac{R_0}{\omega} M_5 e^{i\phi_5} [P_{1R}e^{i\omega(t-z/C_1)}e^{-\delta_1 z/R_0} - P_{2R}e^{i\omega(t+z/C_1)}e^{\delta_1 z/R_0}], \tag{67}$$

$$\xi_R(z, t) = \frac{M_1 e^{i\phi_1}}{\rho\omega^2 R_0} p_R(z, t), \zeta_R(z, t) = \frac{1}{\rho\omega R_0^2}\frac{M_3}{M_5} e^{i(\phi_3-\phi_5)}Q'_R(z, t), \tag{68}$$

$$w_R(0, z, t) = \frac{1}{\rho R_0^2}\frac{M_7}{M_5} e^{i(\phi_7-\phi_5)}Q'_R(z, t). \tag{69}$$

The same equations yield for the second type of wave ($P_{1A} = 0 = P_{2A}$):

$$p_A(z, t) = P_{3A}e^{i\omega(t-z/C_2)}e^{-\delta_2 z/R_0} + P_{4A}e^{i\omega(t+z/C_2)}e^{\delta_2 z/R_0}, \tag{70}$$

$$Q'_A(z, t) = \frac{R_0}{\omega} M_6 e^{i\phi_6} [P_{3A}e^{i\omega(t-z/C_2)}e^{-\delta_2 z/R_0} - P_{4A}e^{i\omega(t+z/C_2)}e^{\delta_2 z/R_0}], \tag{71}$$

$$\xi_A(z, t) = \frac{M_2 e^{i\phi_2}}{\rho\omega^2 R_0} p_A(z, t), \zeta_A(z, t) = \frac{M_4}{M_6} e^{i(\phi_4-\phi_6)}Q'_A(z, t)/\rho\omega R_0^2, \tag{72}$$

$$w_A(0, z, t) = \frac{1}{\rho R_0^2}\frac{M_8}{M_6} e^{i(\phi_8-\phi_6)}Q'_A(z, t). \tag{73}$$

For each type of wave these results show that the radial wall displacement is proportional to the pressure and that the axial wall displacement and fluid velocity on the axis are both proportional to the instantaneous mass flow. Therefore, when only one type of wave and its reflections is admitted to the solution, one may not prescribe independent conditions on pressure and on the radial wall displacements at the same axial location. Similarly it is not permissible to introduce independent

FIGURE 9 The mode shape coefficient M_4 for axial displacement of the second type of wave as a function of α for various values of σ, β_1, β_2, κ_1, and κ_2. For the basic parametric case, M_4 decreases rapidly at small α, attains a minimum, and asymptotically approaches a limit for large α. Poisson's ratio produces a significant variation at most α while a variation in β_1 is of importance only at larger values of α. M_4 is inversely proportional to β_2 when $\lambda_2/R_0 > 1$. Axial displacement for the second type of wave can be markedly decreased by radial constraint at all α. With increasing axial constraint, M_4 increases at small α while at large α it attains a maximum for a certain axial constraint and then decreases.

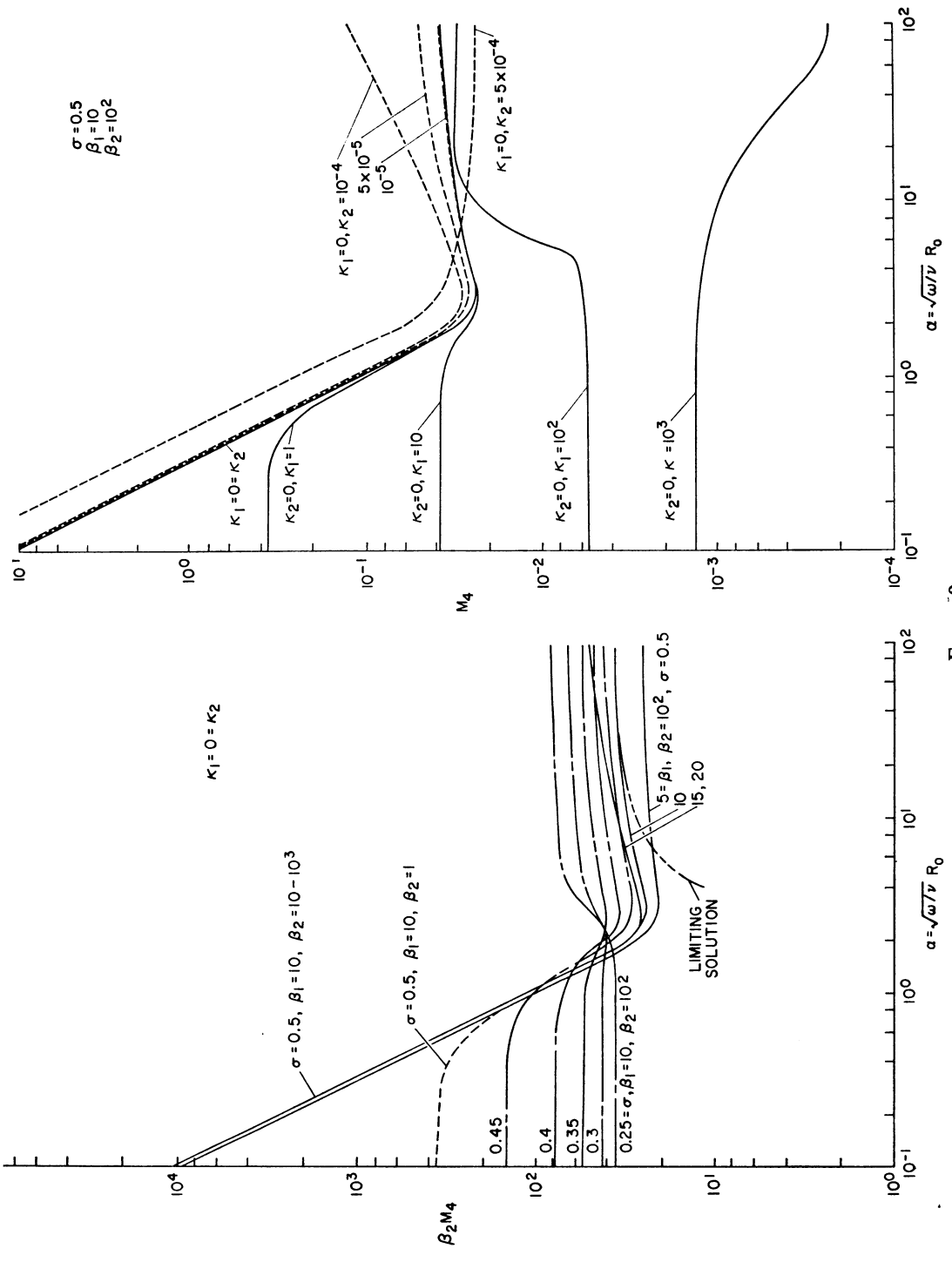
σ=0.5
β1=10
β2=10²
κ1=0=κ2
κ2=0, κ1=1
κ2=0, κ1=10
κ2=0, κ1=10²
κ2=0, κ=10³
κ1=0, κ2=10⁻⁴
5×10⁻⁵
10⁻⁵
κ1=0, κ2=5×10⁻⁴
M4
α=√(ω/ν) R0
κ1=0=κ2
σ=0.5, β1=10, β2=10-10³
σ=0.5, β1=10, β2=1
0.45
0.4
0.35
0.3
0.25=σ, β1=10, β2=10²
5=β1, β2=10², σ=0.5
10
15, 20
LIMITING SOLUTION
β2M4
α=√(ω/ν) R0

FIGURE 9

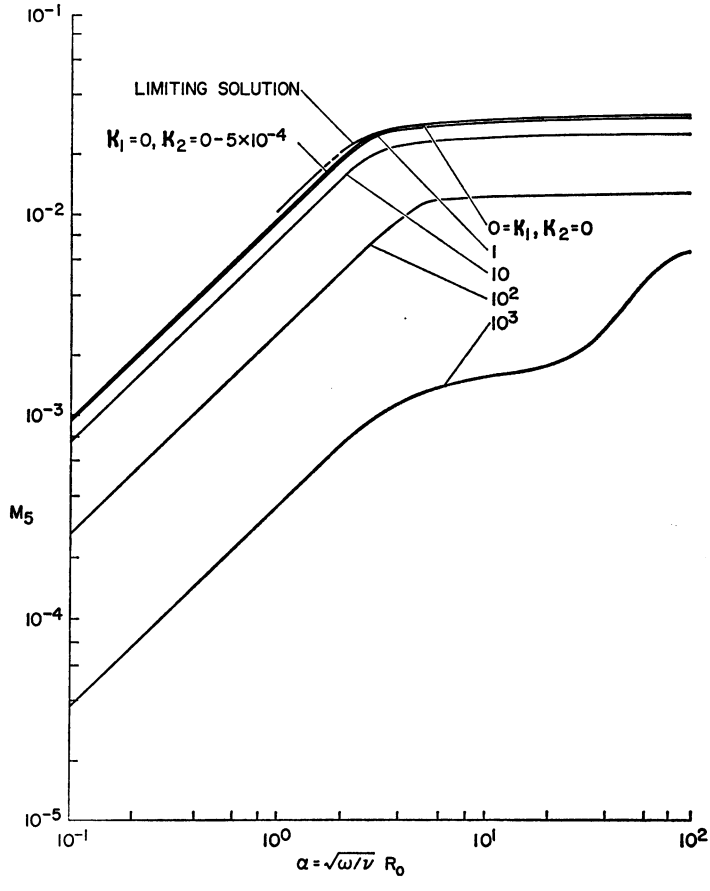

FIGURE 10 The mode shape coefficient M_5 for fluid mass flow rate with the first type of wave as a function of α for different values of the constraint parameters κ_1 and κ_2. M_5 shows no significant dependence upon axial constraint but continuously decreases with increasing radial constraint for all α. M_5 is inversely proportional to the magnitude of the impedance of the first type of wave.

conditions on the instantaneous mass flow, the axial wall displacement, and the fluid velocity on the axis at a given axial location. For the solutions given above (equations 66–69 or 70–73) only two independent conditions are necessary to specify the arbitrary constants.

Further specialization to a single type of wave traveling either in the $+z$ or $-z$ direction leads to wave solutions in which the instantaneous mass flow, the wall displacements, and the fluid velocity on the axis are all proportional to the pressure. Consequently, only one boundary condition is necessary in such cases to determine the motion of the system.

It is important to note that in the past most experimental investigations have attempted to interpret data in terms of only the first type of wave, and in most

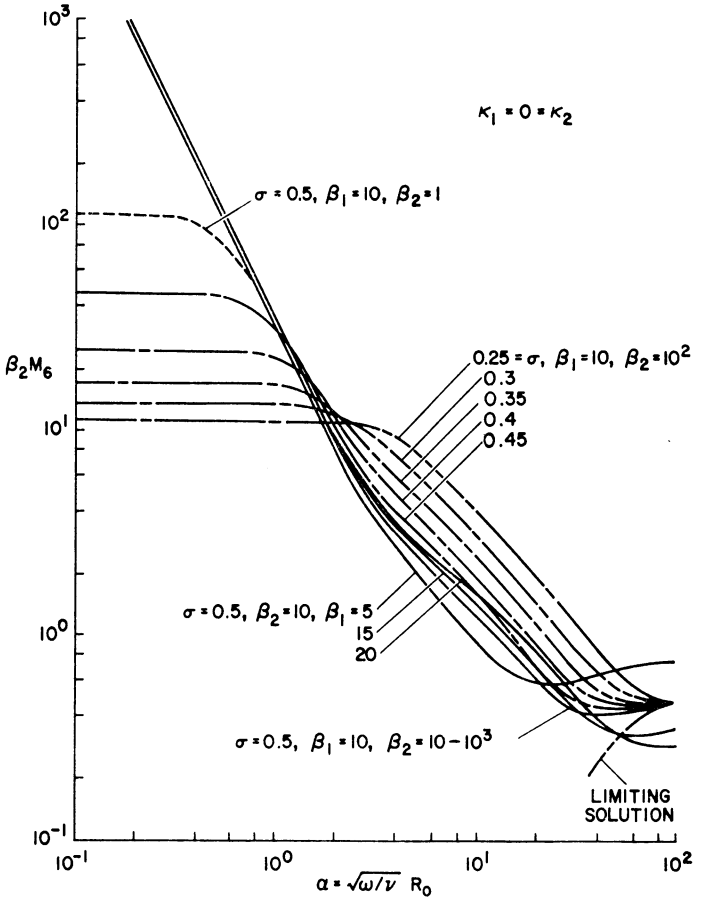

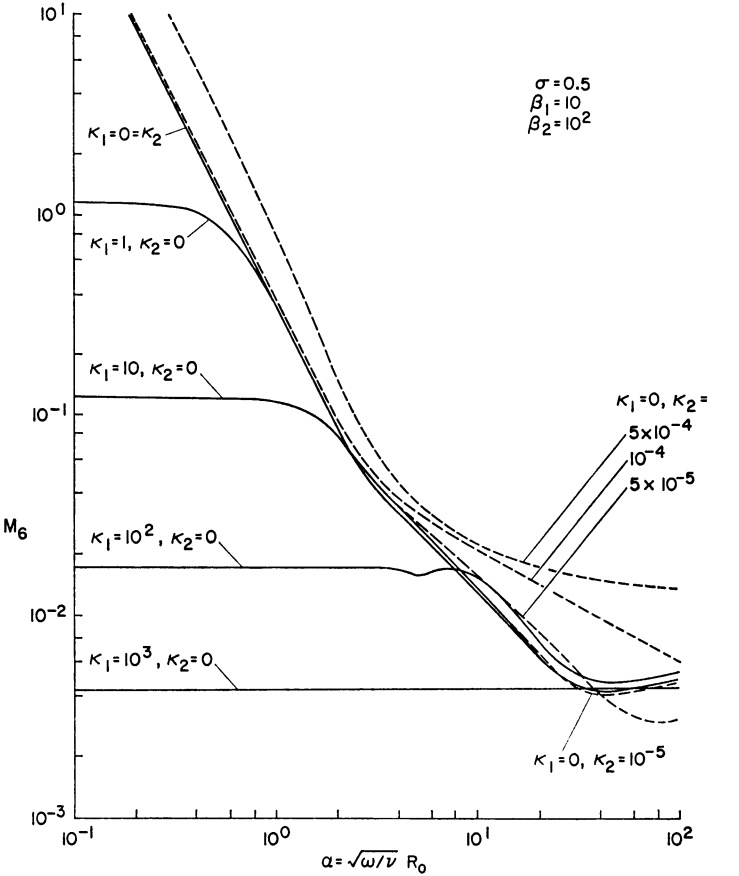

FIGURE 11 The mode shape coefficient M_6 for fluid mass flow rate with the second type of wave as a function of α for various values of the parameters σ, β_1, β_2, κ_1, and κ_2. M_6 exhibits the same trends with variation of σ, β_1, and β_2 as M_2. M_6 is inversely proportional to the magnitude of the impedance of the second type of wave. At all α, M_6 generally decreases with increasing radial constraint and increases with increasing axial constraint.

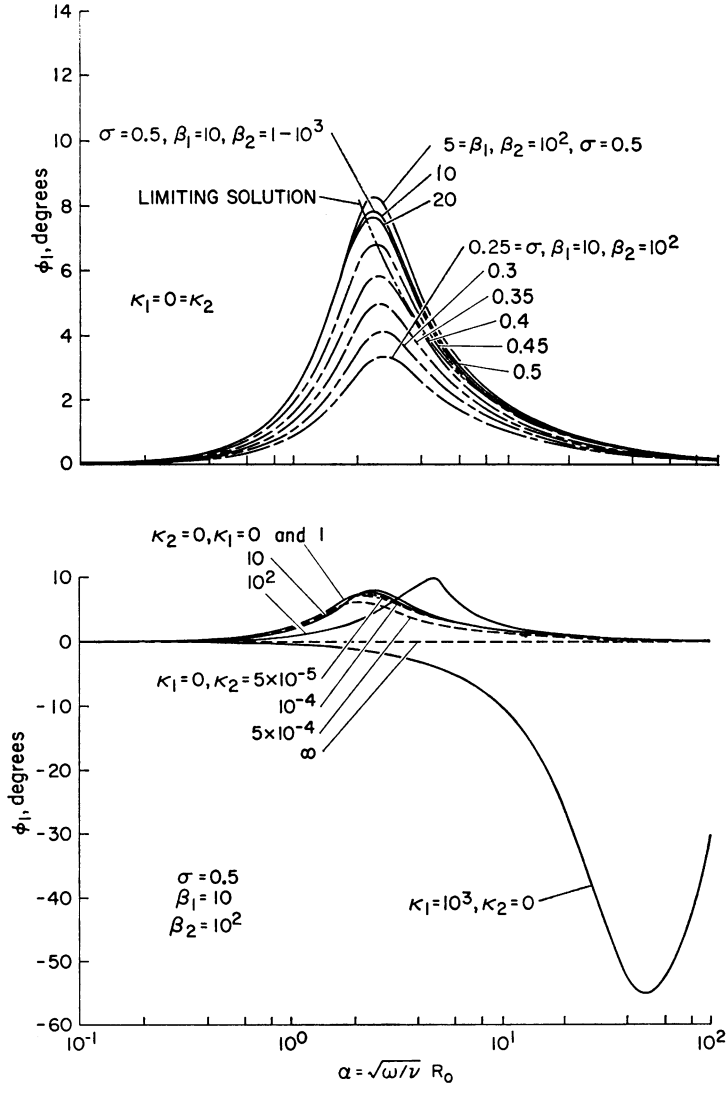

FIGURE 12 The phase angle ϕ_1 for radial displacement of the first type of wave as a function of α for various values of σ, β_1, β_2, κ_1, and κ_2. ϕ_1 is independent of β_2 and assumes a maximum for a value of α independent of σ or β_1; however, the maximum value is small for all parameter values considered here. With increasing axial constraint, ϕ_1 approaches zero for all α. By contrast, as the radial constraint increases, the maximum of ϕ_1 becomes larger and shifts to larger α, but for large radial constraints ϕ_1 assumes a pronounced minimum.

cases the reflected waves (waves traveling in the $-z$ direction) were also neglected. In several of these investigations, however, the experimental apparatus described introduces incompatibilities with the solution that was considered for the wave motion. For example, an electromagnetic flowmeter restricts the radial wall dis-

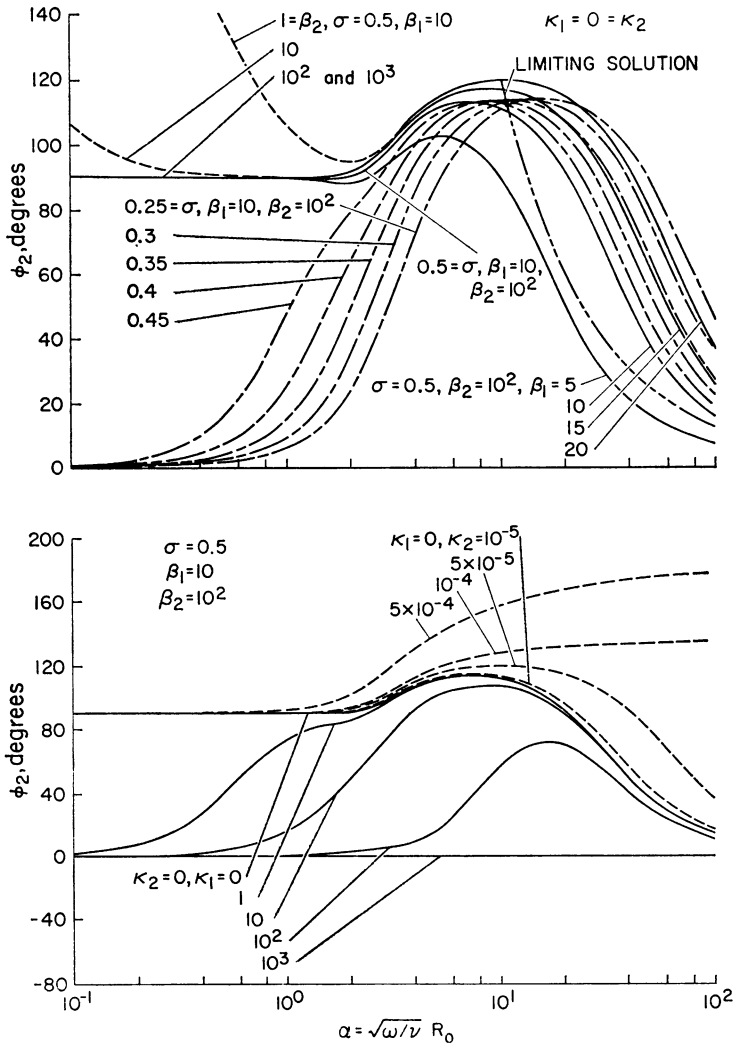

FIGURE 13 The phase angle ϕ_2 for radial displacement of the second type of wave as a function of α for various values of σ, β_1, β_2, κ_1, and κ_2. ϕ_2 is sensitive to changes in σ, β_1, and β_2. Note, however, that it is most sensitive to variations in β_2 for cases where λ_2/R_0 approaches 1. Also, only slight deviation of σ from 0.5 causes a large shift for small α. With increasing axial constraint ϕ_2 increases rapidly, particularly at large α. For increasing radial constraint, ϕ_2 decreases toward 0 with the most rapid decrease at small α.

placement and according to equations 68 and 72 the pressure at that location will be affected.

The parametric analysis demonstrated that the wave propagation characteristics of the second type of wave are more sensitive to physical and geometric system parameters than those of the first type of wave. It is therefore particularly desirable

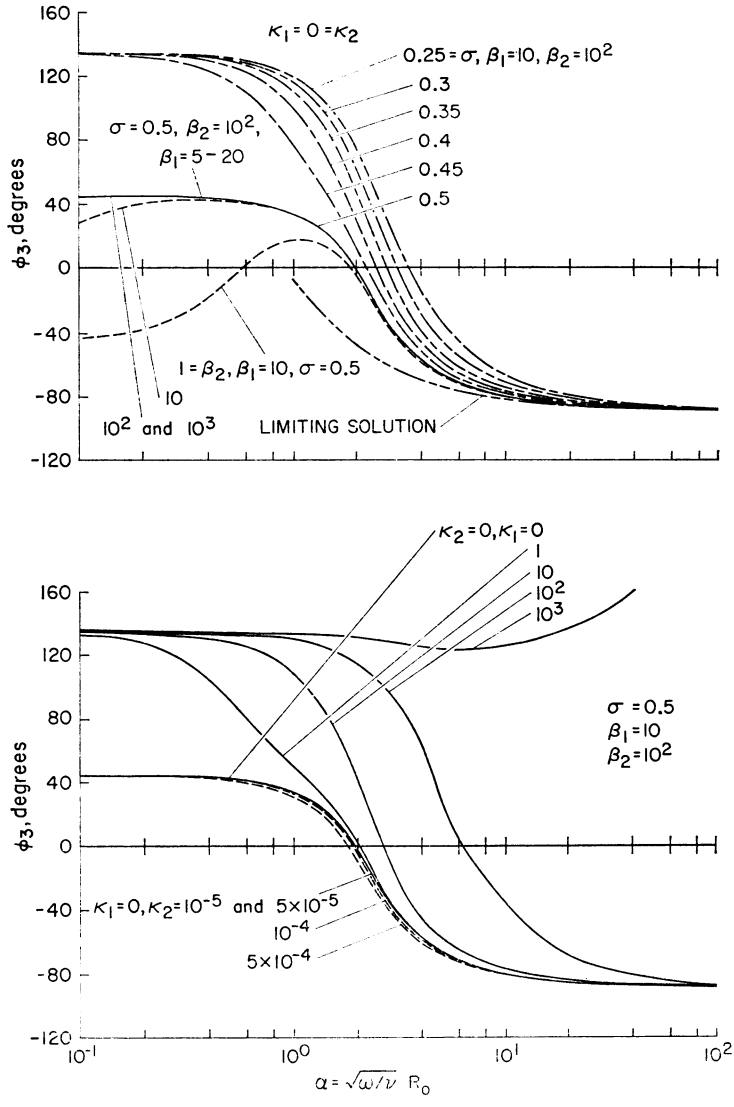

FIGURE 14 The phase angle ϕ_3 for axial displacement of the first type of wave as a function of α with various values of the parameters σ, β_1, β_2, κ_1, and κ_2. ϕ_3 is independent of β_1 and, for all $\beta_2 \geq 100$, it decreases monotonically from the asymptotic limit at low α and approaches asymptotically a lower limit at large α. For smaller β_2, ϕ_3 assumes a relative maximum. At small α, ϕ_3 is generally very sensitive to departures of σ from 0.5. Axial constraints have a mild effect upon ϕ_3 at intermediate values of α while radial constraints increase ϕ_3 markedly.

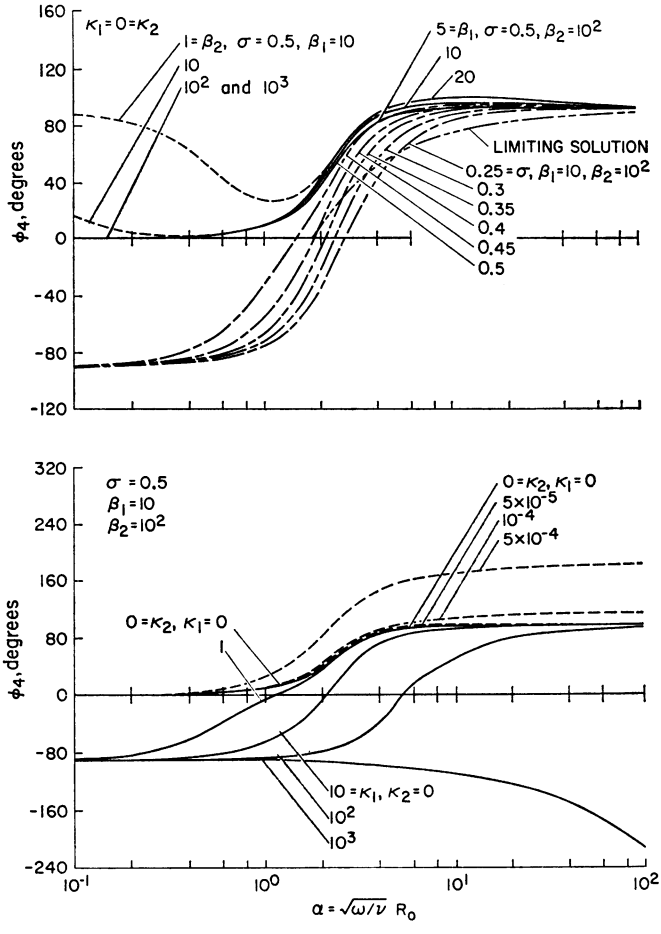

FIGURE 15 The phase angle ϕ_4 for axial displacement of the second type of wave as a function of α for various values of the parameters σ, β_1, β_2, κ_1, and κ_2. Except for $\beta_2 < 100$, ϕ_4 increases from the asymptotic limit at low α toward a limiting value. Significant variations in ϕ_4 can be observed with σ and β_1. ϕ_4 is also very sensitive to departures of σ from 0.5 at small α. ϕ_4 increases with increasing axial constraint, particularly at large α, while it decreases with increasing radial constraint at all α.

to acquire experimental data on the second type of wave when the physical parameters are to be determined from wave transmission characteristics.

V. CONCLUSIONS

The general solution of the boundary value problem posed in this analysis produces two types of waves traveling along the axis of the vessel. The first or slower type of wave has been studied extensively by Womersley and others. Both types have been investigated by several authors (3–5, 16, 19–24), however, without considering the

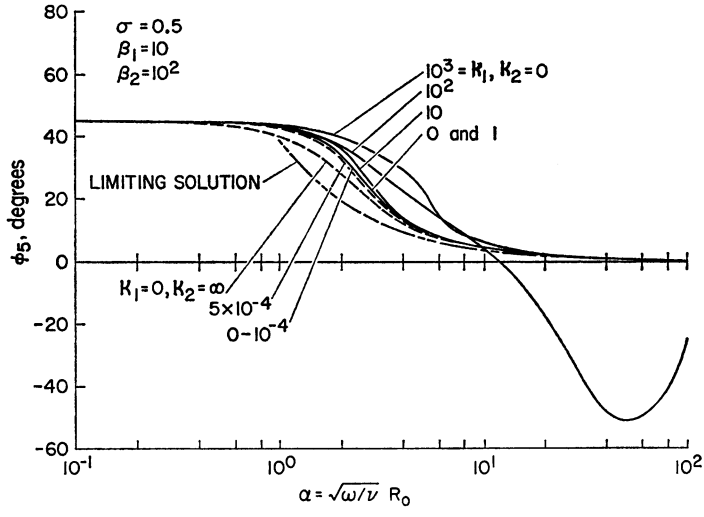

FIGURE 16 The phase angle ϕ_5 for fluid mass flow rate of the first type of wave as a function of α for different values of the constraint parameters κ_1 and κ_2.

effects of constraints. The results of Atabek and Lew (16), Womersley (15), and the present analysis are in good agreement for corresponding values of the system parameters. The analytical predictions given here for the large α limit also corroborate those of Maxwell and Anliker (3–5) for an inviscid fluid.

As in the publications by Womersley (15) and Atabek and Lew (16), the fluid viscosity appears in this investigation only through the nondimensional parameter $\alpha = \sqrt{\omega/\nu}R_0$. A parametric study shows that a variation in α produces the most significant changes in the wave propagation characteristics for the slow waves when $\alpha < 5$ and for the fast waves when $\alpha > 1$. The frequency appears not only in α, but also in the parameter $\beta_2 = C_0/(R_0\omega)$ which plays an important role in determining the mode shapes.

In the presence of a weak radial constraint, the wave speed for the first type of wave (C_1) increases monotonically with α from 0 at $\alpha = 0$ and reaches asymptotically a value which differs by less than 20% from the Moens-Korteweg speed C_0. For the second type of wave with very small values of α and mild distributed external constraints (axial and/or radial) the wave speed (C_2) is relatively insensitive to variations in α. Furthermore, $C_2 = 1.8\ C_0$ for $\alpha < 1$, and with increasing α it approaches an approximate limit value of $5\ C_0$. A distributed radial constraint can produce an order of magnitude variation in C_1 while a distributed axial constraint produces a variation of less than 20%; however, a radial or axial constraint can cause an infinite change in C_2.

Regardless of the constraints, the first or slower type of wave is strongly attenuated for $\alpha < 1$, and the attenuation due to the blood viscosity diminishes rapidly with increasing α. In the absence of constraints the waves of the second or

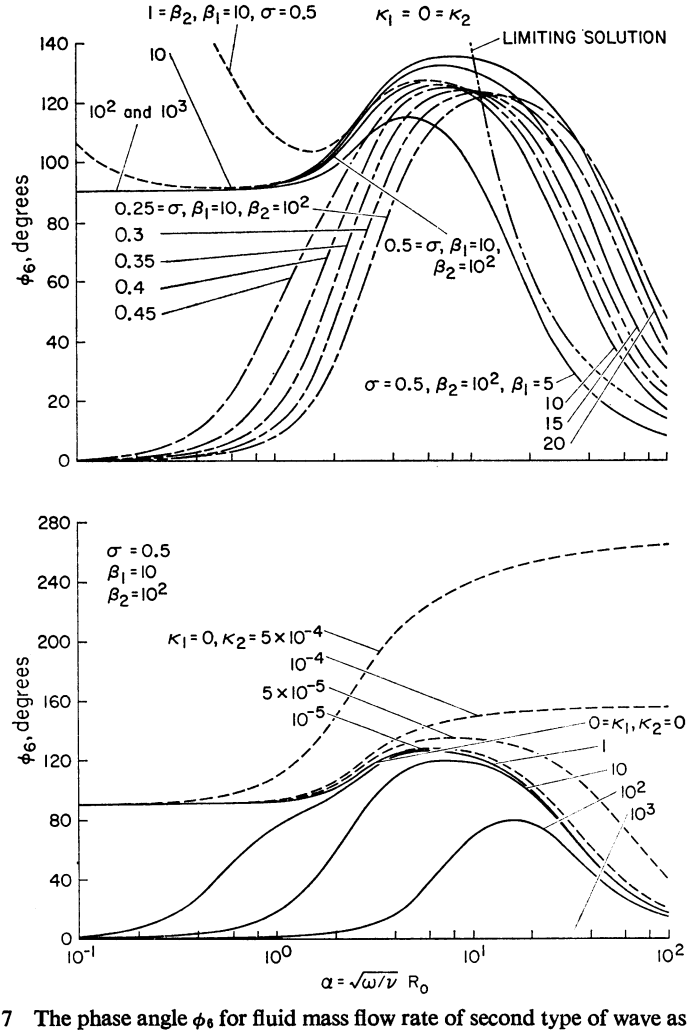

FIGURE 17 The phase angle ϕ_6 for fluid mass flow rate of second type of wave as a function of α for various values of the parameters σ, β_1, β_2, κ_1, and κ_2. ϕ_6 shows the same trends as ϕ_2, the phase angle for radial displacement with this type of wave. Constraints also produce similar effects on ϕ_6 as on ϕ_2.

faster type exhibit a small attenuation due to the viscosity of the blood for $\alpha < 0.2$ and $\alpha > 100$. Their attenuation assumes a maximum for $\alpha \approx 2.8$ and in contrast to the slow waves, is strongly affected by either distributed external constraint.

For the first type of wave the wall displacement has a dominant radial component at high frequencies but at low frequencies the axial displacement component dominates. The second type of wave has a dominant axial displacement component. Both of these statements are true in the presence of weak external constraints. Increasing constraints alter the displacements considerably. The wall motions

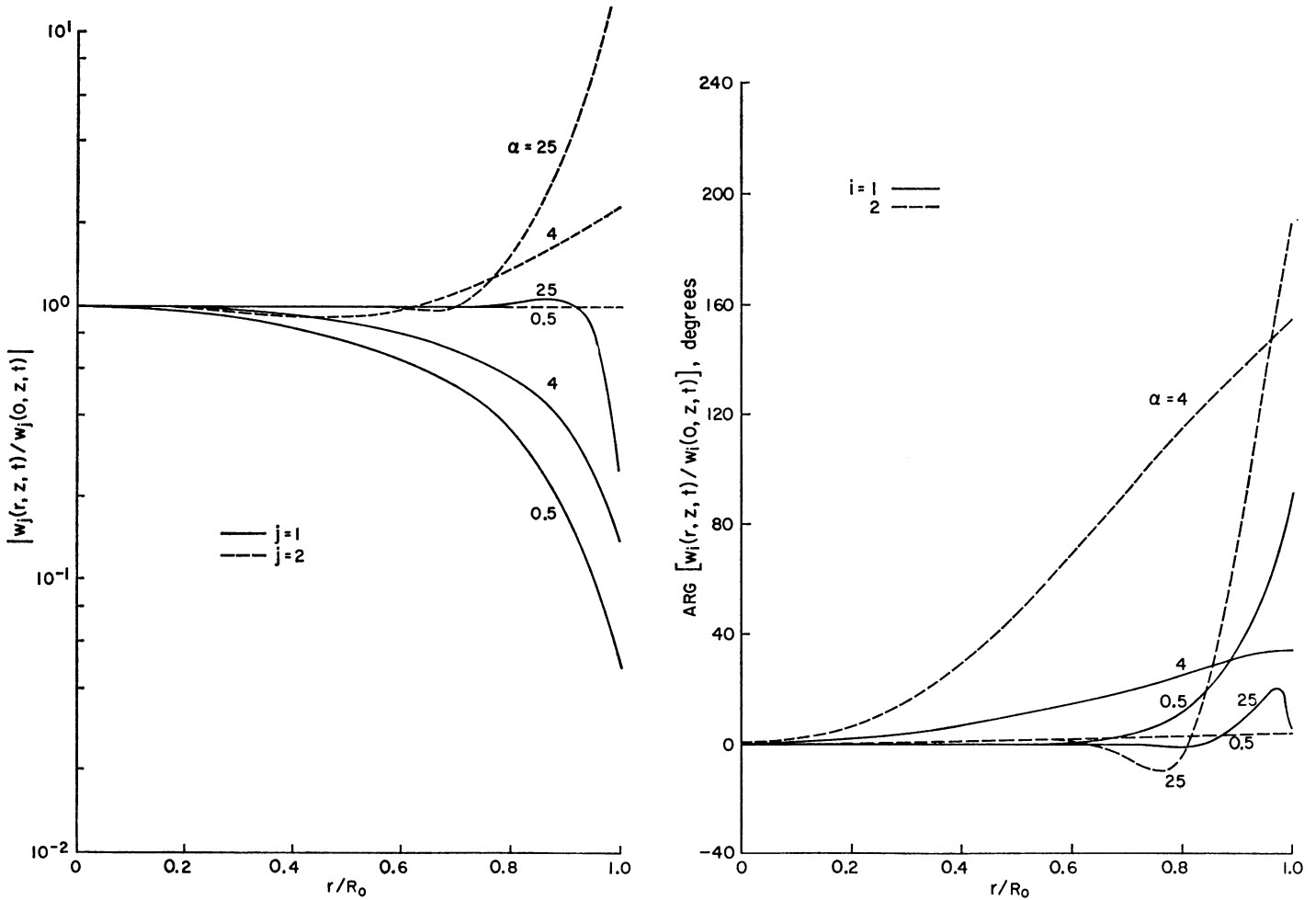

FIGURE 18 Radial distribution of the magnitude and phase for axial fluid velocity.

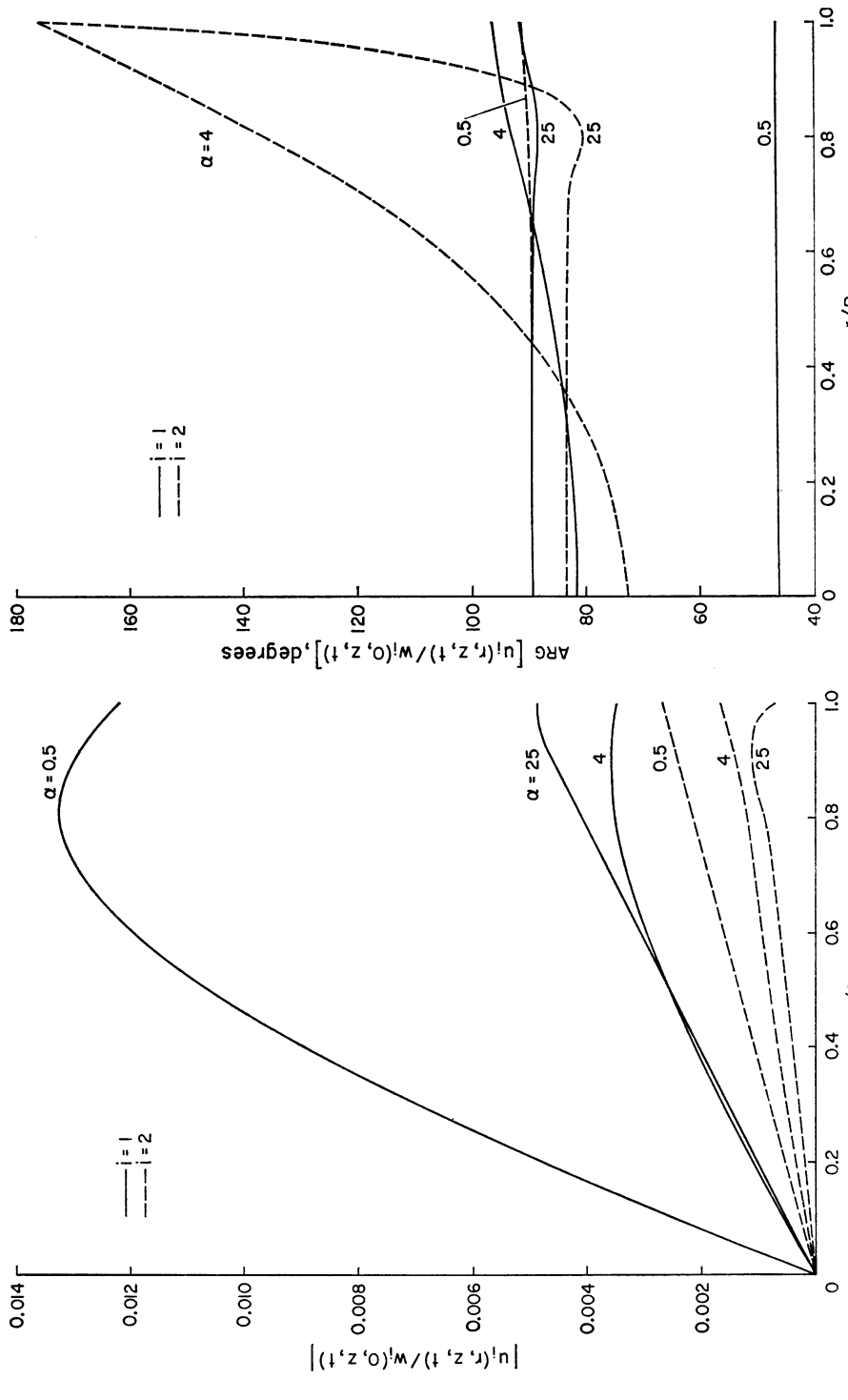

FIGURE 19. Radial distribution of the magnitude and phase for radial fluid velocity.

associated with the two types of waves indicate that the faster type of wave involves a strong shearing interaction between the blood and the vessel wall while the slow type of wave should exhibit relatively strong pressure fluctuations, particularly at higher frequencies.

The second type of wave was found to be much more sensitive to variations in the system parameters than the first type. The phase angles between pressure and radial wall displacement for the first type of wave are almost negligible. An investigation of the effects of discrete constraints such as clamps or electromagnetic flowmeters on the pressure and instantaneous mass flow has demonstrated that such constraints may produce significant effects.

NOMENCLATURE

B_1, B_2 Parameters defined by equation 36.
C_0 Moens-Korteweg wave speed defined in equation 25.
C_1 Wave speed for first type of wave given in equation 42.
C_2 Wave speed for second type of wave given in equation 42.
E Modulus of elasticity for the tube wall.
$F(z)$ An arbitrary function of z.
$F_1(z)$ An arbitrary function of z.
F_2 An arbitrary constant in equation 15.
F_3 An arbitrary constant in equation 30
h Wall thickness.
$\mathbf{i}_n$ Unit vector normal to wall.
$\mathbf{i}_r$ Unit vector in radial direction.
$\mathbf{i}_z$ Unit vector in axial direction.
J_0 Bessel function of first kind of order 0.
J_1 Bessel function of first kind of order 1.
K_1 Proportionality factor for radial constraint.
K_2 Proportionality factor for axial constraint.
L Characteristic axial dimension.
M_1–M_8 Mode shape coefficients defined in equations 49–52.
p Pressure.
P_1–P_4 Arbitrary constants in equation 40.
Q Fluid mass flow rate.
r Radial coordinate.
R_0 Mean radius of the tube.
S_1, S_2 Functions defined by equation 39.
t Time.
u Radial velocity component.
w Axial velocity component.
Y_0 Bessel function of second kind of order 0.
Y_1 Bessel function of second kind of order 1.
z Axial coordinate.
$Z(z)$, $Z_1(z)$ Arbitrary functions of z.
α Parameter defined by equation 25.
β_1, β_2 Parameters defined by equation 24.
β_3 Parameter defined by equation 25.

Γ_1 Radial constraint parameter defined by equation 24.
Γ_2 Axial constraint parameter defined by equation 24.
δ_1, δ_2 Attenuation coefficients defined by equation 42.
ζ Axial wall displacements.
θ Circumferential angle.
κ_1, κ_2 Constraint parameters defined in equation 59.
λ_1 Wavelength for first type of wave.
λ_2 Wavelength for second type of wave.
μ Coefficient of viscosity of fluid.
ν Kinematic viscosity of fluid.
ξ Radial wall displacement.
ρ Fluid density.
ρ_w Wall density.
σ Poisson's ratio for the elastic wall.
τ_{zz}, τ_{rr}, τ_{rz}, $\tau_{\theta\theta}$ Stress components.
ϕ_1–ϕ_8 The phase angles defined by equations 49–52.
ω Circular frequency.
$(\ )_s$ Steady-state quantity.
$(\ )'$ Unsteady component of a system quantity.

This work was carried out at the Ames Research Center of the National Aeronautics and Space Administration under a collaborative arrangement with Stanford University under National Aeronautics and Space Administration grant NGR 05-020-223.

Received for publication 26 June 1969 and in revised form 9 October 1970.

REFERENCES

1. CHIEN, S., S. USAMI, M. TAYLOR, J. L. LUNDBERG, and M. I. GREGERSEN. 1966. *J. Appl. Physiol.* **21**:81.
2. MCDONALD, D. A. 1960. Blood Flow in Arteries. Arnold Ltd., London.
3. MAXWELL, J. A., and M. ANLIKER. 1966. *In* Biomechanics Symposium. Y. C. Fung, editor. American Society of Mechanical Engineers, New York. 47.
4. MAXWELL, J. A., and M. ANLIKER. 1967. Dispersion and Dissipation of Waves in Blood Vessels. Stanford University, SUDAAR Report No. 312, Stanford, Calif.
5. MAXWELL, J. A., and M. ANLIKER. 1968. *Biophys. J.* **8**:920.
6. BERGEL, D. H. 1961. *J. Physiol. (London).* **156**:458.
7. MCDONALD, D. A., and U. GESSNER. 1966. Wave Attenuation in Viscoelastic Arteries. Proceedings of First International Conference on Hemorheology. Pergamon Press Ltd., Oxford, England. 113.
8. MORITZ, W. E. 1969. Transmission characteristics of distension, torsion and axial waves in arteries. Ph.D. Dissertation. Stanford University SUDAAR Report No. 373, Stanford, Calif.
9. KING, A. L. 1957. *In* Tissue Elasticity. J. W. Remington, editor. American Physiological Society, Washington, D.C. 123.
10. PATEL, D. J., and D. L. FRY. 1966. *Circ. Res.* **19**:1011.
11. RUDINGER, G. 1966. *In* Biomedical Fluid Mechanics Symposium. American Society of Mechanical Engineers, New York. 1.
12. SKALAK, R. 1966. Biomechanics Symposium. Y. C. Fung, editor, American Society of Mechanical Engineers, New York. 20.
13. FUNG, Y. C. 1968. *Appl. Mech. Rev.* **21**:1.
14. MORGAN, G. W., and J. P. KIELY. 1954. *J. Acoust. Soc. Amer.* **25**:323.
15. WOMERSLEY, J. R. 1957. An Elastic Tube Theory of Pulse Transmission and Oscillatory Flow in

Mammalian Arteries. WADC Technical Report TR 56-614. Wright Air Development Center, Ohio.
16. ATABEK, H. B., and H. S. LEW. 1966. *Biophys. J.* **6**:481.
17. ATABEK, H. B. 1968. *Biophys. J.* **8**:626.
18. JONES, E. 1968. Effects of viscosity and external constraints on wave transmission in blood vessels. Ph.D. Dissertation. Stanford University, Stanford, Calif. *Diss. Abstr. B.* **29**:2405.
19. ANLIKER, M., W. E. MORITZ, and E. OGDEN. 1968. *J. Biomech.* **1**:235.
20. TAYLOR, M. G. 1959. *Phys. Med. Biol.* **4**:63.
21. KLIP, W. 1962. Velocity and Damping of the Pulse Wave. Martinus Nijhoff, Gravenhague, The Netherlands.
22. KLIP, W., P. VAN LOON, and D. A. KLIP. 1967. *J. Appl. Phys.* **38**:3745.
23. CHOW, J. D. F., and J. T. APTER. 1968. *J. Acoust. Soc. Amer.* **44**:437.
24. COX, R. H. 1969. *J. Biomech.* **2**:251.